EFFECT OF VARIATION OF PRESHEATH IONS TEMPERATURE ON MULTICOMPONENT MAGNETIZED PLASMA-WALL TRANSITION

A Dissertation

Submitted to the Dean Office, Institute of Science & Technology

Tribhuvan University, Kirtipur

in Partial Fulfillment for the Requirement of

Master's Degree of Science in Physics

By

Basanta Raj Dangal

May, 2022

RECOMMENDATION

This is certified that **Mr. Basanta Raj Dangal** has carried out this thesis work entitled **"EFFECT OF VARIATION OF PRESHEATH IONS TEMPERATURE ON MULTICOMPONENT MAGNETIZED PLASMA-WALL TRANSITION"** under our supervision. We recommend the dissertation in the partial fulfillment for the requirement of Master's Degree of Science in Physics at Tribhuvan University, Kirtipur, Kathmandu, Nepal.

. . . . . .

Assoc. Prof. Dr. Lekh Nath Mishra
Patan Multiple Campus, T.U.
Patan Dhoka, Lalitpur,
Nepal

. . . . . .

Mr. Roshan Chalise
Patan Multiple Campus, T.U.
Patan Dhoka, Lalitpur,
Nepal

ACKNOWLEDGEMENTS

At first, I would like to express my sincere gratitude to my supervisors, Assoc. Prof. Dr. Lekh Nath Mishra and Mr. Roshan Chalise for their guidance and motivation with an excellent atmosphere throughout my dissertation. They were so friendly that I never felt any hesitation working with them and doing fruitful discussions during the work. I am extremely thankful to Dr. Suresh Basnet for his coordination and encouragement during this work.

I am grateful to Dr. Lekhanath Mishra, HoD of Physics Department, Patan Multiple Campus and M.Sc. Physics Co-ordinator Dr. Suresh Prasad Gupta for giving a practical framework to complete research work. I am thankful to all the faculty members and staffs of the Physics Department.

Thanks to my friends Mr. Shreekar Tiwari, Mr. Rabi Dahal, Mr. Premhari Lamsal for their valuable time, knowledge and cooperation during this work.

I am thankful to every personality who supported me throughout this work from various places to complete this work smoothly.

Thank you all.

EVALUATION

We certify that we have evaluated this dissertation entitled **"EFFECT OF VARIATION OF PRESHEATH IONS TEMPERATURE ON MULTICOMPONENT MAGNETIZED PLASMA-WALL TRANSITION"** submitted by **Mr. Basanta Raj Dangal** and in our opinion, it fulfills all the specified criteria, in the scope and quality, as a Dissertation for the partial fulfillment of the requirement for the degree of Master's of Science in Physics at Tribhuvan University, Kirtipur, Kathmandu, Nepal.

Evaluation Committee:

Assoc. Prof. Dr. Lekh Nath Mishra
(Head/ Supervisor)
Department of Physics
Patan Multiple Campus, T.U.
Patan Dhoka, Lalitpur, Nepal

Mr. Roshan Chalise
(Supervisor)
Department of Physics
Patan Multiple Campus, T.U.
Patan Dhoka, Lalitpur, Nepal

Dr. Suresh Prasad Gupta
(M.Sc. Co-ordinator)
Department of Physics
Patan Multiple Campus, T. U.
Patan Dhoka, Lalitpur, Nepal

External Examiner

Internal Examiner

Date: .....

ABSTRACT

The characteristics of the magnetized plasma sheath have been studied using the kinetic trajectory simulation method for different ion temperatures of two positive ions. Kinetic equations are solved for a given initial boundary condition to study the effects on electric potential, particle density, electric field, and space charge density of the flow of particle species towards the wall. The electric potential is steeply increasing towards the wall for all the cases and reaches the wall quickly for higher heavier ions' temperatures and slower for equal ions' temperatures. From the sheath entrance, the number density of all particle species decreased, ion density remained maximum for their respective higher ion temperatures, and electron density decreased much faster than positive ions and reached a minimum in all cases. The gap between the value of the electric field in the injection boundary and in the wall is maximum for equal ion temperature of both ions and decreases the difference on increasing any of the two ions' temperatures. This is because a magnetic field dominates near the sheath entrance and an electric field dominates close to the wall. The space charge density is zero at the sheath entrance and it goes on increasing towards the wall to attend its maximum value due to the rapid decrease in electron density. This work gives a brief description of sheath characteristics near the wall, which are useful for multiple plasma applications such as material processing, surface modifications, etching, etc.

CONTENTS

CHAPTER 1

INTRODUCTION

Chapter 1

Introduction

1.1 Introduction to Plasma

Plasma is the form of matter, generally known as the fourth state of matter. When enough temperature is applied to a solid, it changes into a liquid state by breaking down its crystal structure. On the further increasing temperature, it converts into a gas state; finally, given a sufficiently high temperature, the gas is ionized, called plasma. The term 'plasma' was firstly used by Irving Langmuir, the novel laureate who pioneered the scientific study of ionized gases. The word 'Plasma' comes from the Greek '$\pi\lambda\sigma\mu\alpha$', which means something 'moldable substance' or 'jelly' [1]. The first plasma was discovered by Sir William Crookes while experimenting on an electrical discharge tube [2]. In other words, plasma is the ionized quasi-neutral gas of charged and neutral particles that show collective behavior. In this case, collective behavior means the charged particles move around and generate positive and negative charges, which produce electric fields, current and magnetic fields and keep the motion of other charged particles away. Also, the term quasi-neutral means the number density of electrons is almost equal to the number density of ions (i.e., $n_i \approx n_e = n$, where n is for plasma density). Over 95% of the observable matter of universe is made up of plasma such as Star, Nebula, Stellar interiors, atmospheres and entire galaxies can be seen because of their plasma state [3].

The Saha equation tells us about the amount of ionization expected in a gas in thermal equilibrium:

$$\frac{n_i}{n_n} \approx 2.4 \times 10^{21} \frac{T^{3/2}}{n_i} e^{-U_i/KT} \tag{1.1}$$

Where n_i and n_n are the density (number per m^3) of ionized atoms and neutral atoms respectively. T is gas temperature in K^o, K is Boltzmann's constant and U_i is the ionization energy which is amount of energy required to remove outermost electron from an atom.

1.2 Debye Shielding

The system is bounded by the electromagnetic forces and even a small disturbances applied on the system exhibits collective response. This explains collective behavior of the plasma. When external charged particles are imposed to plasma having charged and neutral particles, the same polarity of charge is repelled and opposite polarity charge is attracted to form the spherical cloud. This process creates the potential on the plasma but fundamental characteristic of plasma is its ability to shield out electric potentials that are applied to system. This phenomenon is known as Debye Shielding, and the length or distance of Debye shielding is used to measure the sheath thickness or shielding distance [3]. The schematic representation of Debye shielding is shown in Figure 1.1.

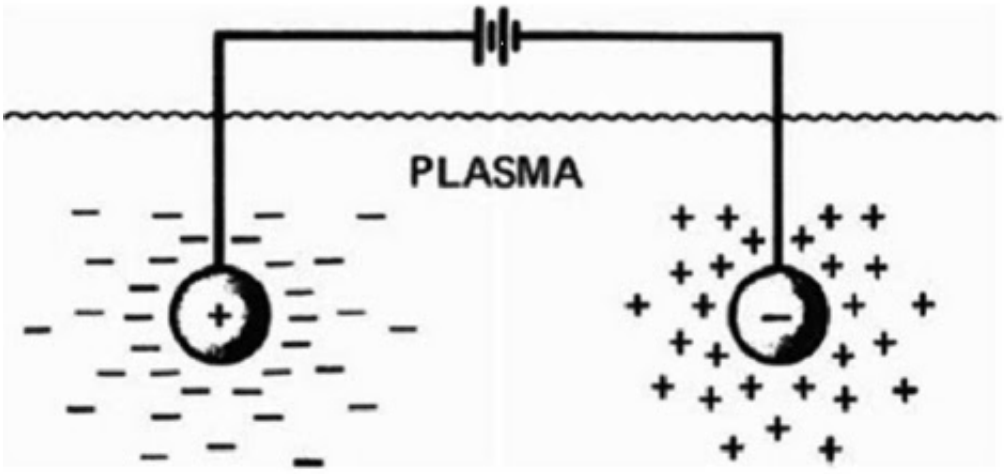

Figure 1.1: Schematic diagram of the Debye shielding [3].

The Debye length is a measurement of the shielding distance i.e. the distance over which effect of any external electric field of an individual charge particle is felt by other charged particle within the plasma. The radius of the Debye sphere is also known as the Debye length. The Debye sphere grows larger as the Debye length increases and the plasma losses its quasineutral and collective

properties resulting in, the plasma behaves as a simply ionized gas. The mathematical expression for the electron Debye length is given by,

$$\lambda_{De} = \sqrt{\frac{\epsilon_0 K_B T_e}{n_0 e^2}} \tag{1.2}$$

where T_e, n_0, ϵ_0, K_B and e are electron temperature, plasma density, permittivity of free space, Boltzmann constant and electronic charge respectively.

From the definition it is known that all ionized gas couldn't be plasma, to be plasma they must fulfill these three conditions:

1) The plasma dimension of the system (L) should be very large as compared to the electron Debye length (λ_{De}), i.e. $\lambda_{De} << L$.

2) In the Debye sphere, the number of particles N_D should be very large, i.e. $N_D >>> 1$. According to this condition, the total number of particles in a Debye sphere should be very large, so that the plasma can shield external potential and can show quasi-neutrality and collective behavior. The shielding would not be statistically valid if there were only a few particles in a Debye sphere. In the Debye sphere, the total number of particles can be calculated as follows:

$$N_D = \frac{4}{3}\pi\lambda_{De}^3 n_0 \tag{1.3}$$

3) Plasma oscillation frequency (ω_{pe}) must be greater than the frequency of electrons colliding with neutral atoms (ω_{en}), i.e. (ω_{pe}) > (ω_{en}). When plasma is abruptly disturbed from its equilibrium state, the resulting internal space charge fields produce collective particle movements that tend to reestablish charge neutrality. These collective motions are characterized by the natural frequency of oscillation known as the plasma frequency. Assume that plasma is initially at rest and is then introduced to an external force. Plasma becomes disturbed due to the imposed external force. When the external force is removed, plasma tends to return to its initial position, while electrons go beyond the equilibrium spot, resulting in an electric field in the opposite direction. This causes the plasma to move in a collective manner. This collective oscillation of the plasma is called plasma frequency. The mathematical expression

for the electron plasma frequency;

$$\omega_{pe} = \sqrt{\frac{n_0 e^2}{\epsilon_0 m_e}} \tag{1.4}$$

where m_e is the mass of an electron.

1.3 Plasma-Wall Transition

The complicated process may be present in the plasma-wall interaction (PWI) phenomenon, which is one of the oldest issues in plasma physics; yet, it attracts substantial or even rising attention and remains an attentive subject for researchers [5–7]. The plasma interacts with the material surface through a non-neutral plasma sheath formed near Plasma Facing Materials (PFMs) and is of great interest in plasma experiments as well as Magnetic Confinement Fusion (MCF) devices such as the International Thermonuclear Experimental Reactor (ITER), where the wall and divertor plate are bombarded by high energetic particle fluxes $(10^{20} - 10^{24})m^{-2}s^{-1}$. Plasma interacts with the material surface via a non-neutral plasma sheath formed near to the surface, and the processes of plasma-wall interaction (PWI) are regulated by PWT parameter fluctuations. Plasma has a wide variety of application in not only fusion experiment but also in various field of science and technology including bio-medicine, material surface modification, electronic industries, and so on.

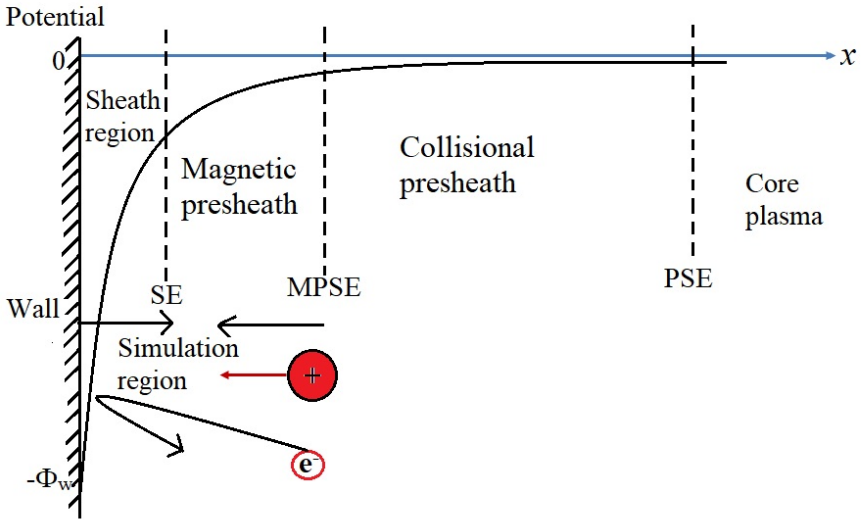

Figure 1.2: Schematic diagram of plasma-wall transition region for magnetized plasma [5].

When plasma comes into contact with a surface or electrode, a spatial region known as the plasma-wall transition (PWT) region exists between the core plasma and the surface or electrode which is divided into two sections: the presheath and the sheath. Figure 1.2 outlines the general structure of the magnetized plasma-wall transition area as well as the mobility of electrons and positive ions in that region. The collisional magnetized presheath area is an adjacent region of core plasma that is divided into two different regions: collisional presheath and magnetic presheath. The presheath region has only collisional presheath in the absence of magnetic field or magnetic field parallel to the normal to the wall, and its scale length is determined by the mean free path of ions, whereas in the case of collisional plasma with oblique magnetic field, the presheath scale length depends on the strength and obliqueness of magnetic field and ion-neutral collision mean free path. When the magnetic field intensity is strong, the typical expansion of the ion Larmor radius has the greatest impact on compressing the collisional presheath [9].The magnetic presheath is the adjacent layer of sheath region and its spatial dimension is in the order of ion Larmor radius [8];

$$\text{Length of magnetic presheath}(L_{\text{MP}}) = \sqrt{6}\frac{c_s}{\omega_{ic}}\sin\theta \tag{1.5}$$

where c_s is the acoustic speed of ions, ω_{ic} is ion cyclotron frequency and θ is the angle made by the magnetic field with the direction of electric field. Figure (1.2) depicts a schematic diagram of the collisional magnetized plasma plasma-wall transition region, where PSE, MPSE and SE stands for the presheath edge, magnetic presheath edge, and sheath edge, respectively.

1.3.1 Sheath and Presheath

Plasma comes into contact with the material surface practically almost in all plasma applications. As the electrons have much higher thermal velocity than positive ions, they are lost much quicker and the plasma ends up with a net positive charge. The plasma must thus have a positive potential with respect to the wall, implying that the wall potential ϕ_w is negative. Because the Debye shielding will constrain the potential variation to a layer of many Debye lengths in thickness, this potential cannot be diffused across the whole plasma. A thin layer that exists in the vicinity of a material wall is called a sheath [3, 4]. The purpose of a sheath is to create a potential barrier so that more mobile species, such as electrons, are electrostatic ally confined. The schematic illustration of the plasma sheath and the motion of charged particles in the sheath region is shown in Figure 1.3.

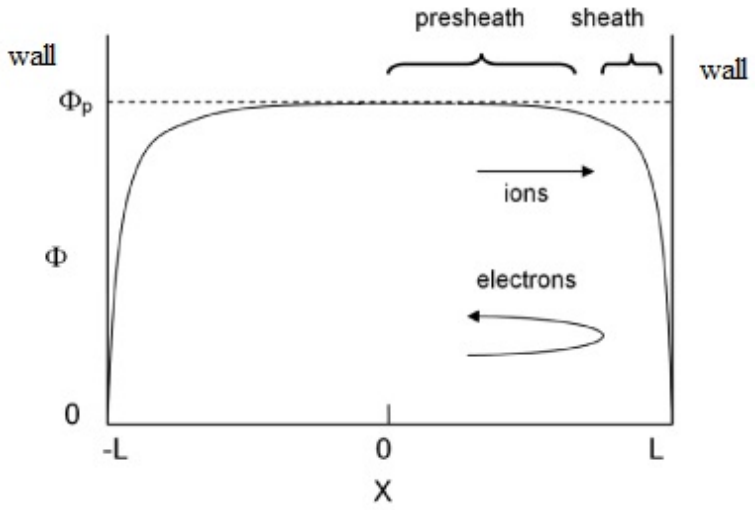

Figure 1.3: Sheath formation near the material walls [3].

Presheath is a transition layer that lies between the sheath and the core plasma and has a longer scale length than a non-neutral plasma sheath [4]. In comparison to the sheath, the potential and other physical parameters in the presheath region has weak gradient. The wall's negative potential has the strongest influence solely in the sheath region; nevertheless, the shielding is not perfect, and the residual electric field penetrates deep into the bulk plasma beyond the sheath edge. The acceleration of ions entering the sheath region is due to the effect of residual electric field at the sheath edge. The monoenergetic ions must enter the sheath region from the presheath side at a velocity greater than the ion-acoustic velocity to form a sheath, which is known as the Bohm sheath condition [7]. Mathematically, the Bohm sheath criterion in the absence of magnetic field or perpendicular to the material surface can be written as

$$u_{i0} \geq C_s \tag{1.6}$$

where u_{i0} represents the average velocity of streaming monoenergetic positive ions and

$$C_s = \sqrt{\frac{\gamma^i K_B T_i + \gamma^e K_B T_e}{m_i}} \tag{1.7}$$

is the ion-acoustic velocity. Here, γ^i and γ^e are the ion and electron polytropic constants respectively, m_i is the mass of ion species and T_i and T_e are the ion and electron temperatures respectively. In the presence of an oblique magnetic field, the Bohm sheath condition equation (1.6) becomes

modified called Bohm-Chodura condition, typically expressed as [8],

$$u_{i0} \geq C_s \cos\theta \tag{1.8}$$

where θ is the angle formed by the magnetic field with perpendicular axis to the wall.

1.4 General Objective

In this work, effect on the magnetized multicomponent plasma sheath is displayed when the presheath temperature of both ions is varied for fixed oblique magnetic field. The method used to solved the equation is kinetic trajectory simulation (KTS) model assuming collisionless, non-neutral and time independent plasma sheath.

CHAPTER 2

LITERATURE REVIEW

Chapter 2

Literature Review

The growing use of plasma in fusion research and importance in technology, the confinement of plasma to finite volume is oldest problems in plasma physics and it is not fully solved yet. Many scientist worked on the problem of sheath formation at the plasma boundary using different model. Lately, multicomponent plasma sheath formation is field of interest for many because of its wide applications including material processing, etching, fusion devices and many more, some of relevant literature on this area are as of follows.

Langmuir studied the interaction of electron and positive ion species on the electrical discharge. The potential distribution in plasma was discovered to determine the ion velocity and , as a result, the rate at which the ion arrives to the sheath Double sheath may arise at the boundary of anode glow when anode of small size is used. The idea of Bohm criterion was applied in that work in an implicit form [6].

Chodura studied the effect of magnetic field on the transition layer between a plasma and an absorbing wall using numerical model which simulates the motion of plasma particles in the electric and magnetic fields for a prescribed particle influx and generalized Bohm's condition for monotonic profile. They obtained the transition layer between a plasma and an absorbing wall is composed of magnetic presheath and electrostatic Debye sheath of several Debye lengths. The magnetic field has insensitive effect on the total potential drop between plasma and wall [8].

Riemann reviewed the Bohm criterion and sheath formation in the limit of small Debye length $\lambda_D \to 0$ on the plasma sheath. In his review article, he explained that Bohm criterion expresses a necessary condition for the formation of stationary sheath in front of negative absorbing wall which is illustrated from simple cold-ion fluid model. The kinetic analysis of the surrounding of the sheath edge showed Bohm criterion is not only for arbitrary ion and electron distributions but also for boundary condition at the wall. Due to sheath edge field singularity smooth matching of the presheath and sheath solutions requires an additional transition layer [9].

Holland et al. examined the sheath formed between magnetized plasma and particle absorbing wall for the case in which the magnetic field intercepts the wall at small angle. Time- independent and 1-D model with all functions varying only in the direction normal to the wall and ions are modeled by a Maxwellian velocity distribution and for electrons the fluid description is used assuming electron-neutral collisions. They found that if $\lambda \leq 1$, the wall potential is negative and the sheath scale length is on the order of ion gyro-radius also if $\lambda \geq 1$ the wall potential is positive and for large λ the sheath is characterized by the short length adjacent to the wall and the ion gyro-radius away from the wall. The potential at the wall is negative close to that of un-magnetized plasma and weakly dependent on ϵ [10].

Shaw et al. observed the properties of magnetized multi-component plasma sheath with finite positive ion temperature. The ion densities, the ion velocities and electric potential inside the sheath are analyzed using three fluid hydrodynamic model and some dimensionless variables. Furthermore, the magnetic field's absence and presence, as well as its orientation, are taken into account. They observed that as positive ion temperature rises, the lighter positive ion density peaks increase only at the sheath edge and shift towards the sheath edge in the absence and presence of a magnetic field. In the absence of a magnetic field, the density peaks at the sheath edge for heavier positive ions. However, in the presence of a magnetic field, density fluctuations at the sheath edge increase. The density peaks shift towards the sheath edge in both cases [11].

Hatami et al. investigated numerical parameters of the magnetized plasma sheath characteristics in the presence of negative ions. By using hydrodynamic approach and ignoring collision and ionization, they shown numerically that by increasing the density of negative ions in the plasma

the density distribution of both positive ions and their kinetic energy decreases and increases respectively and also normalized electrostatic potential in sheath region increases. The numerical results show that decreasing the temperature of the negative ions increases the amplitude of the fluctuations of the net density distribution of the charged particles in the sheath region and shifts their position toward the sheath edge. Finally, it is seen that in the absence of negative ions, the net density distribution of charged particles in the sheath region is monotonic, whereas it is nonmonotonic in the presence of negative ions [12].

Paul et al. worked on sheath formation on weakly magnetized collisionless electronegative plasma using the hydrodynamic equations and assumed electrons and negative ions to follow the Boltzmann relation. They investigated the sheath structure by varying the electronegativity. The presence of negative ions has been found to have a significant effect on the sheath structure and the decrease in the negative ion temperature leads to decrease in electric force. The findings in this paper have far-reaching implications for plasma processing, particularly in the semiconductor industry and fusion research [13].

Masoudi and Khoramabadi investigated the dynamic of a collisional magnetized plasma sheath with two positive ions, in which an external magnetic field and elastic collision between ions and neutrals are taken into account and numerically solved using a plasma fluid model. Given that the collisional frequencies of both ions have a power law dependency on the ions flow speeds, the sheath dynamics are independent near the sheath edge, but increasing the distance from the sheath edge and ions velocity in cathode direction shows sensitiveness to power law dependency [14].

Huiping et al. demonstrated the sheath criterion for electronegative plasma in an oblique magnetic field taking effect of negative ions and external magnetic field on the sheath using theoretical and numerical calculations. Because of Coulomb attraction between positive and negative ions, they discovered that the ion Mach number is relatively low. The ion Mach number is also affected by the magnitude and angle of the magnetic field, as well as the initial velocity of ion flow [15].

Khanal developed a Kinetic Trajectory Simulation (KTS) model for bounded plasma in which the distribution function of the particle species involved is calculated directly by solving the kinetic

equations along the respective collisionless particle trajectories. Exact ion trajectories are used in this method to calculate the ion distribution function assuming a given ion injection distribution at injection. The full velocity distribution of electrons is cut-off Maxwellian due to absorption at the wall. The model is then applied to the single-emitter plasma diode to validate the previous result. Using the same model, the space charge sheath between the absorbing wall and presheath plasma is investigated, and a solution to the presheath sheath coupling problem for a particle moving in a single direction is developed [16].

Chalise investigated the magnetized plasma-wall transition in an oblique magnetic field. Using the KTS model to obtain the final self-consistent solution to a non-neutral, time-independent, collisionless plasma sheath for a given electron and ion density distribution at the sheath entrance. At the magnetic presheath region, the electric field does not exhibit the usual monotony. The magnitude and orientation of the magnetic field have no effect on the plasma parameters reaching the material wall, but they are heavily influenced near the sheath entrance [17].

Basnet and Khanal used kinetic theory to investigate the magnetized plasma sheath characteristics with two species of positive ions. For plasma containing two singly charged positive ions, Bohm's condition has been derived. At the sheath entry, the magnitude of cut-off and Maxwellian maximum velocities is the same, but it increases at the wall as the concentration of second ion species rises. They found that as ion and electron fluxes decrease towards the sheath region of a charged particle, the self-consistent potential profile monotonically decreases towards the wall. The deviation between simulation and theoretical results caused by the cut-off Maxwellian velocity distribution of electrons is less than 0.2 percent in magnitude [18].

Pandey et al. investigated the structure of a plasma sheath in the presence of an oblique magnetic field. The effect of plasma magnetization, plasma ionization and plasma–neutral collisions on the sheath is examined for different orientations of the magnetic field. Inside the sheath, the grains are negatively charged, except near the wall, where they become positively charged. The sheath width is determined not only by the ion-magnetization level, but also by the magnetic field's orientation. When the ion cyclotron frequency is increased by an order of magnitude, the sheath width changes significantly, also by the angle of field orientation [19].

Sharma et al. studied the sheath structure and ion flux to the wall of a collisional magnetized plasma made up of two temperature electrons numerically. The Maxwellian distribution describes low-temperature electrons, while the truncated Maxwellian distribution describes high-temperature electrons. Sheath width and ion flux to the wall have been found to be non-monotonous functions of collision frequency and hot electron concentration. The ion velocity at the sheath edge is determined using an analytically derived sheath formation criterion. With increasing hot electron concentration and temperature, the sheath edge velocity is found to decrease [20].

Basnet et al. studied the effect of presheath electron temperature on plasma-wall interaction mechanism and its consequence on wall sputtering using kinetic simulation method. Multi component plasma interacts with tungsten (W) surface through non-neutral plasma sheath formed near the Plasma Facing Material (PFM) and assuming that two ion species have different temperatures with same degree of ionization. The findings of this work indicates that electron temperature at the presheath-sheath boundary has a significant impact on the angle of incidence at the wall and its sputtering rate [21].

Adhikari et al. studied the transition of coupling parameters from pre-sheath to sheath region using the Kinetic Trajectory Simulation (KTS) method. In this study, the self consistent potential profile as well as the ion temperature in the sheath was shown to be dependent upon the presheath temperature. The variation of Child sheath thickness as well as both electron and ion distribution including the space charge density was studied [22].

Shaw et al. investigated the effect of ion temperature, magnitude magnetic field and its orientation on magnetized multi-component plasma sheath with electron and two species of positive ions. Some dimensionless equation and dimensionless variables obtained during experiment is solved by using three-fluid hydrodynamic model. The significant change in ion densities and energies in sheath is observed with increase of the ion temperature and magnetic field strength. The ion density near the sheath edge increases on increasing magnetic field angle keeping ion temperature constant. Ion density near the sheath is increased for lighter ion species and decreased for heavier ion species near the sheath edge [23].

Chaulagain studied effect of temperature variation in two- ion species in magnetized plasma sheath by using kinetic trajectory simulation. It was found that effect of applied magnetic field is more on ions whereas electrons are non-responsive. The ion density increases on increasing ion temperature but potential decrease in magnitude. Total charge density and also the ion density increases on increasing ion temperature [24].

2.1 Specific Objectives

The specific objectives of this work are:

1) to study the plasma sheath formation for different cases for different temperature of ions,

2) to study the change in space charge density from entrance to wall.

CHAPTER 3

Methodology

Chapter 3

Methodology

3.1 Kinetic Trajectory Simulation Model

Single-particle motion, kinetic theory and fluid theory are three major theoretical methods for studying the plasma properties. In single-particle theory, describing the plasma behavior is challenging because the plasma densities are in the intermediate range (10^{14} m^{-3}). If one of the particles follow the complex trajectory, the prediction of plasma behavior would be the impossible task. Collective effects are frequently unimportant in the single particle theory. The kinetic theory describes plasma properties based on the particle distribution function in which the measurable macroscopic behaviour of system can be measured by averaging over the distribution function. The fluid model describes macroscopic plasma dynamics using differential equations that take into account macroscopic average parameters including density, flux, velocity, pressure, temperature, and heat flux, etc. The identity of a single particle is ignored in fluid theory, and only the motion of the fluid element is considered. The fluid model described majority of plasma phenomena and also known as the simplest description of plasma. There are some phenomena, for which a fluid treatment is inadequate. For these, we need to consider the velocity distribution function $f(\mathbf{v})$ for each species, this treatment is called kinetic theory. In this method, the distribution function of particles can be calculated by solving the kinetic equations along the collision less trajectories of respective particle species [3]. Here we assume the electron and ion velocity distribution functions at the sheath edge to be shifted cut-off Maxwellian.

KTS is an iterative method for numerically calculating self consistent, time-independent kinetic plasma states in some given bounded spatial region. The details of KTS method is discussed in the

previous works [5, 16, 17, 22]. The plasma states are generally characterized by

1. Velocity distribution function *f(**r**, **v**, t)*
2. Electric field **E(r)**
3. Magnetic field **B(r)**
4. Given boundary conditions

The distribution function is the function prescribing the instantaneous density of particles in phase-space and is denoted by $f(\mathbf{r}, \mathbf{v}, t)$. Therefore, $f(\mathbf{r}, \mathbf{v}, t)d\mathbf{r}d\mathbf{v}$ is the number of particles at time t having positions in the range between $\mathbf{r}$ and $\mathbf{r} + d\mathbf{r}$ and velocities in the range between $\mathbf{v}$ and $\mathbf{v} + d\mathbf{v}$. As time progresses, the particle motion and acceleration causes the number of particles in these $\mathbf{r}$ and $\mathbf{v}$ ranges to change and so f will change. In the general case of time-dependent, collisional kinetic theory, the Boltzmann equation for the particle species-s is:

$$\frac{df^s}{dt} = \left(\frac{\partial}{\partial t} + v \cdot \frac{\partial}{\partial \boldsymbol{r}} + \boldsymbol{a}^s \cdot \frac{\partial}{\partial \boldsymbol{v}}\right) f^s = c^s \tag{3.1}$$

where

$$\boldsymbol{a}^s(\boldsymbol{r}, \boldsymbol{v}, t) = \frac{q^s}{m^s}[\boldsymbol{E}(\boldsymbol{r}, t) + \boldsymbol{v} \times \boldsymbol{B}(\boldsymbol{r}, t)] \tag{3.2}$$

is the macroscopic acceleration of species-s particles, $\boldsymbol{E}(\boldsymbol{r})$ and $\boldsymbol{B}(\boldsymbol{r})$ are the macroscopic electric and magnetic fields and c^s is the species-s collision term. For collisionless case, the above equation (3.1) becomes 'Vlasov equation'

$$\frac{df^s}{dt} = \left(\frac{\partial}{\partial t} + v \cdot \frac{\partial}{\partial \boldsymbol{r}} + \boldsymbol{a}^s \cdot \frac{\partial}{\partial \boldsymbol{v}}\right) f^s = 0 \tag{3.3}$$

Obviously, above equation (3.3) gives that for an observer moving along a colisionless species-s trajectory, the species-s kinetic equation is just an ordinary first order differential equation with respect to time zero i.e.

$$\frac{df^s}{dt} = 0 \tag{3.4}$$

implies

$$f^s = constant \tag{3.5}$$

This means that the velocity distribution function is constant for an observer moving along a collisionless trajectory. Hence, the distribution function at every point along the trajectory can be obtained if its value at one point is known.

3.2 Basic Equations

Generalizing Vlasov equation for time-independent, collisionless, 1d3v electrostatic problems leads to following basic differential equations.

(a) For Electron ($q = -e$)

The Vlasov equation for electron with time independent velocity distribution function is,

$$\frac{df^e}{dt} = \left[\mathbf{v}\cdot\nabla - \frac{e}{m^e}\left(\mathbf{E}(\mathbf{r}) + \mathbf{v}\times\mathbf{B}(\mathbf{r})\frac{\partial}{\partial\mathbf{v}}\right)\right] f^e(\mathbf{r},\mathbf{v}) = 0 \tag{3.6}$$

and in trajectory integrated forms as

$$f^e(\mathbf{r},\mathbf{v}) = f^e_{st}\left(\mathbf{r}^e_{st},\mathbf{v}^e_{st}\right) \tag{3.7}$$

where f^e_{st} is the 'starting distribution', $\mathbf{r}^e_{st}$ is the 'starting position and $\mathbf{v}^e_{st}$ is the 'starting velocity' of electron.

The equations of motion for electron are:

$$\frac{d\boldsymbol{r}^{\mathrm{e}}}{dt} = \boldsymbol{v}^{\mathrm{e}} \tag{3.8}$$

with components of velocity

$$\begin{aligned}\frac{dx^{\mathrm{e}}}{dt} &= v^{\mathrm{e}}_x\\ \frac{dy^{\mathrm{e}}}{dt} &= v^{\mathrm{e}}_y\\ \frac{dz^{\mathrm{e}}}{dt} &= v^{\mathrm{e}}_z\end{aligned} \tag{3.9}$$

and

$$\frac{dv^{\mathrm{e}}}{dt} = a^{e} \tag{3.10}$$

with components of acceleration

$$\begin{aligned}
\frac{dv_x^{\mathrm{e}}}{dt} &= a_x^{\mathrm{e}} \\
\frac{dv_y^{\mathrm{e}}}{dt} &= a_y^{\mathrm{e}} \\
\frac{dv_z^{\mathrm{e}}}{dt} &= a_z^{\mathrm{e}}
\end{aligned} \tag{3.11}$$

The macroscopic acceleration of electron is

$$\boldsymbol{a}^{\mathrm{e}}(\boldsymbol{r}) = -\frac{e}{m^{\mathrm{e}}}[\boldsymbol{E}(\boldsymbol{r}) + \boldsymbol{v} \times \boldsymbol{B}(\boldsymbol{r})] \tag{3.12}$$

with its components

$$\begin{aligned}
\boldsymbol{a}^{\mathrm{e}}(\boldsymbol{x}) &= -\frac{e}{m^{\mathrm{e}}}[\boldsymbol{E}(\boldsymbol{x}) + (\boldsymbol{v} \times \boldsymbol{B}(\boldsymbol{x}))_x] \\
\boldsymbol{a}^{\mathrm{e}}(\boldsymbol{y}) &= -\frac{e}{m^{\mathrm{e}}}[\boldsymbol{E}(\boldsymbol{y}) + (\boldsymbol{v} \times \boldsymbol{B}(\boldsymbol{y}))_y] \\
\boldsymbol{a}^{\mathrm{e}}(z) &= -\frac{e}{m^{\mathrm{e}}}[\boldsymbol{E}(z) + (\boldsymbol{v} \times \boldsymbol{B}(z))_z]
\end{aligned} \tag{3.13}$$

(b) For first ion ($q = e$)

The Vlasov equation for singly ionized lighter ion species with time independent velocity distribution function is,

$$\frac{df^1}{dt} = \left[\mathbf{v} \cdot \nabla + \frac{e}{m^1}\left(\mathbf{E}(\mathbf{r}) + \mathbf{v} \times \mathbf{B}(\mathbf{r})\frac{\partial}{\partial \mathbf{v}}\right)\right] f^1(\mathbf{r}, \mathbf{v}) = 0 \tag{3.14}$$

and in trajectory integrated forms as

$$f^1(\mathbf{r}, \mathbf{v}) = f_{st}^1\left(\mathbf{r}_{st}^1, \mathbf{v}_{st}^1\right) \tag{3.15}$$

where f_{st}^1 is the 'starting distribution', $\mathbf{r}_{st}^1$ is the 'starting position and $\mathbf{v}_{st}^1$ is the 'starting velocity' of first ion.

The equations of motion for lighter ion are:

$$\frac{d\boldsymbol{r}^1}{dt} = \boldsymbol{v}^1 \tag{3.16}$$

with components of velocity

$$\begin{aligned} \frac{dx^1}{dt} &= v_x^1 \\ \frac{dy^1}{dt} &= v_y^1 \\ \frac{dz^1}{dt} &= v_z^1 \end{aligned} \tag{3.17}$$

and

$$\frac{dv^1}{dt} = a^1 \tag{3.18}$$

with components of acceleration

$$\begin{aligned} \frac{dv_x^1}{dt} &= a_x^1 \\ \frac{dv_y^1}{dt} &= a_y^1 \\ \frac{dv_z^1}{dt} &= a_z^1 \end{aligned} \tag{3.19}$$

The macroscopic acceleration of first ion is

$$\boldsymbol{a}^1(\boldsymbol{r}) = \frac{e}{m^1}[\boldsymbol{E}(\boldsymbol{r}) + \boldsymbol{v} \times \boldsymbol{B}(\boldsymbol{r})] \tag{3.20}$$

with its components

$$\begin{aligned} \boldsymbol{a}^1(\boldsymbol{x}) &= \frac{e}{m^1}[\boldsymbol{E}(\boldsymbol{x}) + (\boldsymbol{v} \times \boldsymbol{B}(\boldsymbol{x}))_x] \\ \boldsymbol{a}^1(\boldsymbol{y}) &= \frac{e}{m^1}[\boldsymbol{E}(\boldsymbol{y}) + (\boldsymbol{v} \times \boldsymbol{B}(\boldsymbol{y}))_y] \\ \boldsymbol{a}^1(z) &= \frac{e}{m^1}[\boldsymbol{E}(z) + (\boldsymbol{v} \times \boldsymbol{B}(z))_z] \end{aligned} \tag{3.21}$$

(c) For second ion ($q = e$)

The Vlasov equation for singly ionized heavier ion species with time independent velocity distri-

bution function is,

$$\frac{df^2}{dt} = \left[\mathbf{v}\cdot\nabla + \frac{e}{m^2}\left(\mathbf{E}(\mathbf{r}) + \mathbf{v}\times\mathbf{B}(\mathbf{r})\frac{\partial}{\partial\mathbf{v}}\right)\right] f^2(\mathbf{r},\mathbf{v}) = 0 \tag{3.22}$$

and in trajectory integrated forms as

$$f^2(\mathbf{r},\mathbf{v}) = f^2_{st}\left(\mathbf{r}^2_{st},\mathbf{v}^2_{st}\right) \tag{3.23}$$

where f^2_{st} is the 'starting distribution', $\mathbf{r}^2_{st}$ is the 'starting position and $\mathbf{v}^2_{st}$ is the 'starting velocity' of second ion.

The equations of motion for lighter ion are:

$$\frac{d\boldsymbol{r}^2}{dt} = \boldsymbol{v}^2 \tag{3.24}$$

with components of velocity

$$\begin{aligned}\frac{dx^2}{dt} &= v^2_x\\ \frac{dy^2}{dt} &= v^2_y\\ \frac{dz^2}{dt} &= v^2_z\end{aligned} \tag{3.25}$$

and

$$\frac{dv^2}{dt} = a^2 \tag{3.26}$$

with components of acceleration

$$\begin{aligned}\frac{dv^2_x}{dt} &= a^2_x\\ \frac{dv^2_y}{dt} &= a^2_y\\ \frac{dv^2_z}{dt} &= a^2_z\end{aligned} \tag{3.27}$$

The macroscopic acceleration of heavier ion is

$$\boldsymbol{a}^2(\boldsymbol{r}) = \frac{e}{m^2}[\boldsymbol{E}(\boldsymbol{r}) + \boldsymbol{v}\times\boldsymbol{B}(\boldsymbol{r})] \tag{3.28}$$

with its components

$$\begin{aligned} \boldsymbol{a}^2(\boldsymbol{x}) &= \frac{e}{m^2}[\boldsymbol{E}(\boldsymbol{x}) + (\boldsymbol{v} \times \boldsymbol{B}(\boldsymbol{x}))_x] \\ \boldsymbol{a}^2(\boldsymbol{y}) &= \frac{e}{m^2}[\boldsymbol{E}(\boldsymbol{y}) + (\boldsymbol{v} \times \boldsymbol{B}(\boldsymbol{y}))_y] \\ \boldsymbol{a}^2(\boldsymbol{z}) &= \frac{e}{m^2}[\boldsymbol{E}(\boldsymbol{z}) + (\boldsymbol{v} \times \boldsymbol{B}(\boldsymbol{z}))_z] \end{aligned} \tag{3.29}$$

(d) For electric field

The electric field is calculated by using this formula,

$$\mathbf{E}(\mathbf{r}) = -\frac{d\emptyset(\mathbf{x})}{dr} = -\nabla\emptyset(\mathbf{r}) \tag{3.30}$$

where the electrostatic potential $\emptyset(\mathbf{r})$ is to be calculated from the Poisson's equation. The Poisson's equation is

$$\frac{d^2\emptyset(\mathbf{r})}{d\mathbf{r}^2} = -\frac{\rho(\mathbf{r})}{\epsilon_0} \tag{3.31}$$

where ϵ_0 is the permittivity of free space and $\rho(x)$ is the space charge density.

(e) Space Charge Density

The space charge density is calculated as,

$$\rho(\mathbf{r}) = \sum_s q^s n^s \left(\mathbf{r}_j\right) \tag{3.32}$$

and

$$\rho(\mathbf{r}) = e\left[n^1 + n^2 - n^e\right] \tag{3.33}$$

(f) Electron and ion densities

The electron and ion densities given as,

$$n^s(\mathbf{r}) = \int_{-\infty}^{\infty} d^3v f^s(\mathbf{r}, \mathbf{v}), \qquad s = (e, 1, 2) \tag{3.34}$$

These equations are solved for the given field and particle boundary conditions iteratively.

3.3 Description of Model

Our point of interest is to understand the sheath properties of two positive ion species in magnetized plasma sheath for which we made our model as simple as possible and clearly understandable. For simplicity we assume 1d3v (i.e. one dimensional in configuration and three dimensional in velocity space) plasma model which is shown in the figure below. The magnetic field is considered perpendicular to the wall. The plasma region is bounded by two parallel planes located at $x = 0$ is left hand boundary (i.e. wall or electrodes) and $x = L$ is right hand boundary (i.e. sheath entrance) and the plasma consists of only electrons and ion of two species, one of lighter and another of heavier (in our simulation lighter is Oxygen ion and heavier is Argon ion).

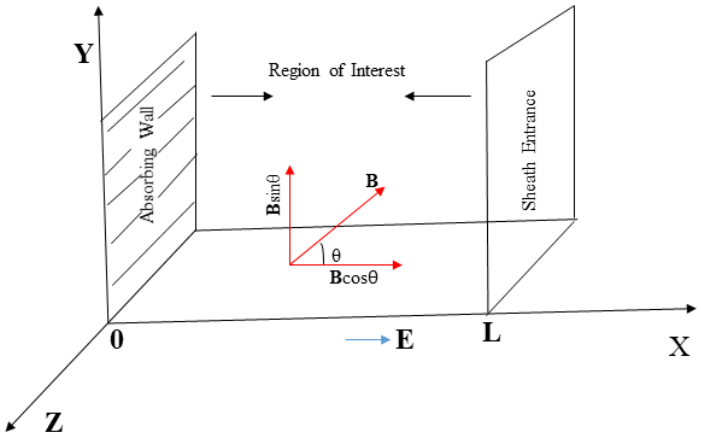

Figure 3.1: Geometrical diagram of magnetized plasma sheath model

Here the right hand boundary is the region from where our sheath region starts which is also called the sheath entrance which generally separates our the collisionless and non-neutral sheath region from the bulk plasma and in the left hand region there is absorbing wall. The angle between an oblique magnetic field along with the X-axis and denoted by θ. Here electric field is along X-axis. For simplicity, consider the plasma parameter vary only along x-direction. The resultant magnetic field is

$$B = B_0[\cos\theta\dot{x} + \sin\theta\dot{y}] \tag{3.35}$$

Hence, in this case the plasma sheath is collisionless time independent and electrostatic.

3.4 Boundary Conditions

To solve the set of equations compiled in Sec. (3.2), we need to know the boundary conditions for the velocity distribution functions (particle boundary conditions) and the potential (field boundary conditions) at the two boundaries of the simulation region. The boundary potentials $\phi(x = 0)$ and $\phi(x = L)$, the boundary injection distribution function $f^s(L, \mathbf{v})$, and the distribution function at the wall $f^s(0, \mathbf{v})$, are assumed to be given. Hence, they must be specified before the iteration is started and are kept constant throughout the entire simulation.

(a) Particle Boundary Conditions

We assume here the plasma particle enters the simulation region from the right-hand boundary with cut-off Maxwellian velocity distributions functions, the left-hand boundary does not emit any particle and that both boundaries are perfectly absorbing. Due to this, the distribution function satisfies the following boundary conditions at the left-hand boundary.

$$f^e(x = 0, \mathbf{v} \leq 0) = 0 \qquad and \qquad f^s(x = 0, \mathbf{v} < 0) = 0, \quad s = (1, 2) \tag{3.36}$$

and at the right-hand boundary,

$$\begin{aligned} f^e(x = L, v \leq 0) &= A^e \exp\left[-\left(\frac{m^e\left(v_x^2 + v_y^2 + v_x^2\right)}{2kT_f^c}\right)\right] \\ f^e(x = L, v \leq 0) &= A^e \exp\left[-\left(\frac{v_x^2 + v_y^2 + v_x^2}{\left(v_{tf}^e\right)^2}\right)\right] \end{aligned} \tag{3.37}$$

and

$$\begin{aligned} f^1(x = L, v < 0) &= A^1 \exp\left[-\frac{m^1\left[\left(v_x^1 - v_{mL}^1\right)^2 + \left(v_y^1\right)^2 + \left(v_z^1\right)^2\right]}{2kT_f^1}\right]\Theta\left(v_{cL}^1 - v_x^1\right) \\ f^1(x = L, v < 0) &= A^1 \exp\left[-\left(\frac{\left[\left(v_x^1 - v_{mL}^1\right)^2 + \left(v_y^1\right)^2 + \left(v_z^1\right)^2\right.}{\left(v_{tf}^1\right)^2}\right)\right]\Theta\left(v_{cL}^1 - v_x^1\right) \end{aligned} \tag{3.38}$$

$$f^2(x=L, v<0) = A^2 \exp\left[-\frac{m^2\left[\left(v_x^2 - v_{mL}^2\right)^2 + \left(v_y^2\right)^2 + \left(v_x^2\right)^2\right]}{2kT_f^2}\right]\Theta\left(v_{cL}^2 - v_x^2\right)$$

$\Theta\left(v_{cL} - v_x\right)$ is the Heaviside function whose value is 1 if $x \geq 0$ and zero otherwise.

$$f^2(x=L, v<0) = A^2 \exp\left[-\left(\frac{\left[\left(v_x^2 - v_{\mathrm{mL}}^2\right)^2 + \left(v_y^2\right)^2 + \left(v_z^2\right)^2\right.}{\left(v_{tf}^2\right)^2}\right)\right]\Theta\left(v_{cL}^2 - v_x^2\right) \tag{3.39}$$

at the right-hand boundary, where T_f^e and T_f^1 and T_f^2 are the thermal temperatures of electron ion of first species and ion of second species respectively.

The thermal velocity given by,

$$v_{tf}^s = \sqrt{\frac{2kT_f^s}{m^s}} \tag{3.40}$$

$s = (e, 1, 2), 1$ and 2 are ion species, v_{mL}^1 and v_{mL}^2 are the ions Maxwellian-maximum velocity at $x = L$. Also v_{cL}^1 and v_{cL}^1 (with $v_{cL}^1 < 0, v_{cL}^2 < 0$) are the ions cut-off velocity at $x = L$. As we assume the electrons enter at injection plane with half Maxwellian and our potential profile is decreasing monotonically towards the left-hand boundary. So, the electron velocity distribution function is given by,

$$f^e(x, \mathbf{v}) = A^e \exp\left[-\left(\frac{v_x^2 + v_y^2 + v_z^2}{\left(v_{tf}^e\right)^2}\right) + \frac{e\phi(x)}{kT_f^e}\right]\Theta\left(v_{cL}^c(x) - v_x\right) \tag{3.41}$$

where,

$$v_c^e(x) = \sqrt{\frac{2e\left[\phi(x) - \phi_o\right]}{m^e}} \tag{3.42}$$

is the electron cut-off velocity at point x.

For $x = L$, in particular we have,

$$f^e(x=L, \mathbf{v}) = A^e \exp\left[-\left(\frac{v_x^2 + v_y^2 + v_z^2}{\left(v_{tf}^e\right)^2}\right)\right]\Theta\left(v_{cL}^e - v_x\right) \tag{3.43}$$

where,

$$v_{cL}^{e} = \sqrt{\frac{-2e\phi_o}{m^e}} \tag{3.44}$$

Similarly, from eq.(3.38) and eq. (3.39) and using the fact that our potential profile is monotonically decreasing towards the wall or electrode and ions enter the sheath entrance with cut-off Maxwellian velocity distribution function, we get the total velocity distribution function at $x = L$ as

$$f^1(x = L, \mathbf{v}) = A^1 \exp\left[-\left(\frac{\left(v_x^1 - v_{mL}^1\right)^2 + \left(v_y^1\right)^2 + \left(v_x^1\right)^2}{\left(v_{tf}^1\right)^2}\right)\right]\Theta\left(v_{cL}^1 - v_x^1\right) \tag{3.45}$$

and

$$f^2(x = L, \mathbf{v}) = A^2 \exp\left[-\left(\frac{\left(v_x^2 - v_{mL}^2\right)^2 + \left(v_y^2\right)^2 + \left(v_x^2\right)^2}{\left(v_{tf}^2\right)^2}\right)\right]\Theta\left(v_{cL}^2 - v_x^2\right) \tag{3.46}$$

In the right-hand side of the Eq.(3.43), Eq.(3.45) and Eq.(3.46), there are eleven parameters, $A^e, T_f^e, v_{cL}^e, A^1, A^2, T_f^1, T_f^2, v_{mL}^1, v_{mL}^2, v_{cL}^1$ and v_{cL}^2 which must be specified according to the physical situation considered. Now the particle density and other physical parameters at $x = L$ are given by

$$\begin{aligned} n_L^e &= \int_{-\infty}^{+\infty} d^3v f^e(L, \mathbf{v}) \\ n_L^1 &= \int_{-\infty}^{+\infty} d^3v f^1(L, \mathbf{v}) \\ n_L^2 &= \int_{-\infty}^{+\infty} d^3v f^2(L, \mathbf{v}) \end{aligned} \tag{3.47}$$

For the velocity distribution given by Eq.(3.43), we evaluate Eq.(3.47) for electron case. The electron density at $x = L$ is

$$\begin{aligned} n_L^e &= \int_{-\infty}^{\infty} d^3v f^e(L, \mathbf{v}) \\ &= \int_{-\infty}^{\infty} dv_x \int_{-\infty}^{\infty} dv_y \int_{-\infty}^{\infty} dv_z A^x exp\left[-\left(\frac{\left(v_x^2 + v_y^2 + v_x^2\right)}{\left(v_{tf}^e\right)^2}\right)\right]\Theta\left(v_{cL}^e(x) - v_x\right) \end{aligned} \tag{3.48}$$

$$n_L^e = A^e \int_{-\infty}^{v_{cL}^e} dv_x \in xp\left[-\left(\frac{v_x}{v_{if}^e}\right)^2\right] \int_{-\infty}^{\infty} dv_{y\in xp}\left[-\left(\frac{v_y}{v_{if}^e}\right)^2\right] \int_{-\infty}^{\infty} dv_x \exp\left[-\left(\frac{v_x}{v_{tf}^e}\right)^2\right] \quad (3.49)$$

Using $\left(\frac{v_x}{v_{tf}^e}\right) = \xi$, we get

$$n_L^e = A^e \int_{-\infty}^{\frac{v_{tf}}{n_{tf}}} d\xi v_{tf}^e \exp\left(-\xi^2\right) d\xi \times \sqrt{\Pi\left(v_{tf}^e\right)^2} \times \sqrt{\Pi\left(v_{if}^e\right)^2} \quad (3.50)$$

$$\begin{aligned} &= A^e \Pi\left(v_{tf}^e\right)^3 \left[\frac{\sqrt{\pi}}{2} + \frac{\sqrt{\pi}}{2} \operatorname{erf}\left(\frac{v_{cL}^e}{v_{tf}^e}\right)\right] \\ &= \frac{\pi^{(3/2)}\left(v_{tf}^e\right)^3 C^e A^e}{2} \end{aligned} \quad (3.51)$$

where,

$$\begin{aligned} C^e\left(T_f^e, \phi_o\right) &= 1 + \operatorname{erf}\left(\frac{v_{cL}^e}{v_{tf}^e}\right) \\ &= 1 + \operatorname{erf}\sqrt{\frac{-e\phi_o}{kT_f^e}} \end{aligned} \quad (3.52)$$

and 'erf' represents the "error function" which is defined as

$$\operatorname{erf}(x) = \frac{2}{\sqrt{\pi}} \int_0^x d\xi \exp\left(-\xi^2\right) \quad (3.53)$$

Now, from the velocity distribution function, eq.(3.45) and eq.(3.47), we get ion density as,

$$\begin{aligned} n_L^1 &= \int_{-\infty}^{+\infty} d^3 v f^1(L, \mathbf{v}) \\ &= \int_{-\infty}^{+\infty} d^3 v A^1 \exp\left[-\left(\frac{\left(v_x^1 - v_{mL}^1\right)^2 + \left(v_y^1\right)^2 + \left(v_x^1\right)^2}{\left(v_{tf}^1\right)^2}\right)\right] \Theta\left(v_{cL}^1 - v_x^1\right) \\ &= \int_{-\infty}^{\infty} dv_x \int_{-\infty}^{\infty} dv_y \int_{-\infty}^{\infty} dv_x A^1 \exp\left[-\left(\frac{\left(v_x^1 - v_{mL}^1\right)^2 + \left(v_y^1\right)^2 + \left(v_x^1\right)^2}{\left(v_{tf}^1\right)^2}\right)\right] \Theta\left(v_{cL}^1(x) - v_x^1\right) \end{aligned} \quad (3.54)$$

$$n_L^1 = A^1 \int_{-\infty}^{v_1^1} dv_x \exp\left[-\left(\frac{v_x^1 - v_{mL}^1}{v_{tf}^1}\right)^2\right] \int_{-\infty}^{\infty} dv_y \in xp\left[-\left(\frac{v_y^1}{v_{tf}^1}\right)^2\right] \int_{-\infty}^{\infty} dv_x \exp\left[-\left(\frac{v_z^1}{v_{tf}^1}\right)^2\right] \tag{3.55}$$

Using $\left(\frac{v_x^1 - v_{mL}^i}{v_{tf}^1}\right) = \xi$, then limit:
At $v_x^1 = -\infty, \xi = -\infty$ and
At $v_x^1 = v_{cL}^1, \xi = \frac{v_{cL}^1 - v_{mL}^1}{v_{tf}^1}$

$$n_L^1 = A^1 \int_{-\infty}^{\frac{v_{cL}^1 - v_{mL}^1}{v_{tf}^1}} d\xi v_{tf}^1 \exp\left(-\xi^2\right) d\xi \times \sqrt{\Pi\left(v_{tf}^1\right)^2} \times \sqrt{\Pi\left(v_{tf}^1\right)^2} \tag{3.56}$$

$$\begin{aligned} &= A^1 \Pi\left(v_{tf}^1\right)^3 \left[\frac{\sqrt{\pi}}{2} + \frac{\sqrt{\pi}}{2} \operatorname{erf}\left(\frac{v_{cL}^1}{v_{tf}^1}\right)\right] \\ &= \frac{\pi^{(3/2)}\left(v_{tf}^1\right)^3 C^1 A^1}{2} \end{aligned} \tag{3.57}$$

where, $C^1 = 1 + \operatorname{erf}\left(\tau_{cL}^1\right)$ and $\tau_{cL}^1 = \left(\frac{v_{cL}^1 - v_{mL}^1}{v_{tf}^1}\right)$

Similarly, from the velocity distribution function, eq.(3.46) and eq.(3.47) for second ion case, we get ion density as,

$$\begin{aligned} n_L^2 &= \int_{-\infty}^{+\infty} d^3 v f^2(L, \mathrm{v}) \\ &= \int_{-\infty}^{+\infty} d^3 v A^2 \exp\left[-\left(\frac{\left(v_x^2 - v_{mL}^2\right)^2 + \left(v_y^2\right)^2 + \left(v_x^2\right)^2}{\left(v_{if}^2\right)^2}\right)\right] \theta\left(v_{cL}^2 - v_x^2\right) \\ &= \int_{-\infty}^{\infty} dv_x \int_{-\infty}^{\infty} dv_y \int_{-\infty}^{\infty} dv_x A^2 \exp\left[-\left(\frac{\left(\left(v_x^2 - v_{mL}^2\right)\right)^2 + \left(v_y^2\right)^2 + \left(v_z^2\right)^2}{\left(v_{Lf}^2\right)^2}\right)\right] \Theta\left(v_{cL}^2(x) - v_x^2\right) \end{aligned} \tag{3.58}$$

$$n_L^2 = A^2 \int_{-\infty}^{v_\alpha^2} dv_x \exp\left[-\left(\frac{v_x^2 - v_{mL}^2}{v_{if}^2}\right)^2\right] \int_{-\infty}^{\infty} dv_y \in xp\left[-\left(\frac{v_y^2}{v_{tf}^2}\right)^2\right] \int_{-\infty}^{\infty} dv_x \exp\left[-\left(\frac{v_z^2}{v_{tf}^2}\right)^2\right] \tag{3.59}$$

Using $\left(\frac{v_x^2 - v_{mL}^2}{v_{tf}^2}\right) = \xi$, then limit:
At $v_x^2 = -\infty, \xi = -\infty$ and
At $v_x^2 = v_{cL}^2, \xi = \frac{v_{cL}^2 - v_{mL}^2}{v_{tf}^2}$

$$n_L^2 = A^2 \int_{-\infty}^{\frac{v_{cL}^2 - v_{mL}^2}{v_{tf}^2}} d\xi v_{tf}^2 \exp\left(-\xi^2\right) d\xi \times \sqrt{\Pi\left(v_{tf}^2\right)^2} \times \sqrt{\Pi\left(v_{tf}^2\right)^2} \tag{3.60}$$

$$= A^2 \Pi\left(v_{tf}^2\right)^3 \left[\frac{\sqrt{\pi}}{2} + \frac{\sqrt{\pi}}{2} \in rf\left(\frac{v_{cL}^2}{v_{tf}^2}\right)\right] \tag{3.61}$$

$$= \frac{\pi^{(3/2)\left(v_{tf}^2\right)^3} C^2 A^2}{2} \tag{3.62}$$

where, $C^2 = 1 + \text{erf}\left(\tau_{cL}^2\right)$ and $\tau_{cL}^2 = \left(\frac{v_{cL}^2 - v_{mL}^2}{v_{tf}^2}\right)$. We can also define the "complementary error function" as

$$\text{erf}\, c(x) = 1 - \text{erf}(x) \tag{3.63}$$

(b) Field Boundary Conditions

The potential profile at $x = L$ is chosen as zero, whereas the one at $x = 0$ is fixed to a negative constant value, i.e.

$$\begin{aligned} \phi(x = 0) &= \phi_o = \text{ const. } < 0 \\ \phi(x = L) &= \phi(L) \\ &= 0 \end{aligned} \tag{3.64}$$

We restrict ourselves to the potential distribution which decreases monotonically from $x = L$ to

$x = 0$ such that the electric field is always negative.

3.5 Solution of Poisson's Equation

After the calculation of the electron and ion densities from numerical integration the space charge density distribution can be obtained using

$$\begin{aligned} \rho\left(x_j\right) &= \sum_s q^s n^s\left(x_j\right) \\ &= e\left[z_1 n^1\left(x_j\right) + z_2 n^2\left(x_j\right) - n^e\left(x_j\right)\right] \end{aligned} \tag{3.65}$$

where z_1 and z_2 are the ionization ratio for first and second species. Here in our case these ionization ratio is taken as one. By the knowing the space charge distribution, $\rho\left(x_j\right)$, from eq. (3.65) we can solve the Poisson's eq.(3.31) numerically to obtain the related new potential distribution, $\phi\left(x_j\right)$. The discretized form of Poisson's equation is given by

$$\frac{\phi_{j+1} - 2\phi_j + \phi_{j-1}}{(\Delta x)^2} = -\frac{\rho_j}{\epsilon_o} \tag{3.66}$$

Now we write this equation for all internal grid points in the simulation region ($j = 2, 3, \ldots, n_x - 1$) which yields the following $n_x - 2$ equations involving n_x unknowns, $\phi_1, \phi_2, \ldots., \phi_{n_x}$:

$$\phi_1 - 2\phi_2 + \phi_3 = -\frac{(\Delta x)^2}{\epsilon_o}\rho_2 \tag{3.67}$$

$$\phi_2 - 2\phi_3 + \phi_4 = -\frac{(\Delta x)^2}{\epsilon_o}\rho_2 \tag{3.68}$$

$$\phi_{n_x-2} - 2\phi_{n_x-1} + \phi_{n_x} = -\frac{(\Delta x)^2}{\epsilon_o}\rho_{n_x-1} \tag{3.69}$$

We have fixed the potential values at the two boundaries as

$\phi(x = L) = \phi_{n_x} = \phi_L$

and

$\phi(x = 0) = \phi_1 = \phi_0$

By solving the eq. (3.67), eq. (3.68) and eq. (3.69) we now obtain the potential distribution, i.e. the potential values $\phi_1, \phi_2, \ldots., \phi_{n_x}$ which can be expressed as a single matrix equation as

$$\begin{pmatrix} 1 & 0 & 0 & 0 & . & . & 0 \\ 1 & -2 & 1 & 0 & . & . & 0 \\ 0 & 1 & -2 & . & . & . & 0 \\ . & . & . & . & . & . & . \\ . & . & . & . & . & . & . \\ . & . & . & . & 1 & -2 & 1 \\ . & . & . & . & 0 & 0 & 1 \end{pmatrix} \times \begin{pmatrix} \phi_1 \\ \phi_2 \\ . \\ . \\ . \\ \phi_{n_x-1} \\ \phi_{n_x} \end{pmatrix} = \begin{pmatrix} \phi_o \\ -\frac{(\Delta x)^2}{\epsilon_o}\rho_2 \\ . \\ . \\ . \\ -\frac{(\Delta x)^2}{\epsilon_o}\rho_{n_x-1} \\ \phi_L \end{pmatrix} \tag{3.70}$$

The matrix on the left-hand side and the one at the right-hand side are known. In order to solve the matrix equation inverse of the first matrix is multiplied with the right-hand side matrix which is done using a simple command in MATLAB program.

Relaxation Scheme

The exact solution of Poisson's equation converges only for short systems (a few Debye lengths). As the system length increases, small fluctuation of the potential causes nonphysical accumulation of the charges and the scheme breaks down. To overcome this difficulty we use the relaxation scheme. The numerically exact potential distribution function $\phi_e x^{(m)}(x_j)$ obtained by numerically solving eq. (3.70) is linearly combined with old potential distribution $\phi^{(m-1)}(x_j)$ to obtain the "re-adjusted" new potential distribution function $\phi^{(m)}(x_j)$, which is actually used as the relevant result of the m^{th} iteration:

$$\phi^{(m)}(x_j) = \omega\phi_e x^m + (1-\omega)\phi^{(m-1)}(x_j) \tag{3.71}$$

with $0 < \omega < 2$.

3.6 Electric Field Calculation

Here in this section we are going to discuss how the electric field is calculated at all the grid points from a given potential profile, and how the field is calculated for the points lying between two grid points.

(a) Electric Field at the Inner Grid Points:

At the inner grid points $j = 1, 2, \ldots\ldots\ldots, n_x - 1$, the electric field is obtained as,

$$E(x) = -\frac{\phi\left(x_{j+1}\right) - \phi\left(x_{j-1}\right)}{2\Delta x} \tag{3.72}$$

(b) Electric Field at the Left-Hand Boundary:

Near the left-hand boundary $(x = 0)$ we assume, for the potential, the parabolic approximation as,

$$\phi(x) = \phi_1 + ax + bx^2 \tag{3.73}$$

where $\phi_0 = \phi_1$ is the potential at $x = 0$. For the second and third grid points, we have the two equations

$$\phi_2 = \phi_1 + a\Delta x + b(\Delta x)^2 \tag{3.74}$$

and

$$\phi_3 = \phi_1 + 2a\Delta x + 4b(\Delta x)^2 \tag{3.75}$$

respectively, from which the constants ' a ' and ' b ' can be obtained as

$$a = -\frac{3\phi_1 - 4\phi_2 + \phi_3}{2\Delta x} \tag{3.76}$$

and

$$b = \frac{\phi_1 - 2\phi_2 + \phi_3}{2(\Delta x)^2} \tag{3.77}$$

the electric field near $x = 0$ is obtained by taking the derivative of eq. 3.73 as

$$\begin{aligned} E(x) &= -\frac{d\phi(x)}{dx} \\ &= -a - 2bx \end{aligned} \tag{3.78}$$

So that the electric field at the left-hand boundary is given by

$$\begin{aligned} E(x=0) &= -a \\ &= \frac{3\phi_1 - 4\phi_2 + \phi_3}{2\Delta x} \end{aligned} \tag{3.79}$$

(c) Electric Field at the Right-Hand Boundary:

Near the right-hand boundary $(x = L)$, we assume for the potential the parabolic approximation as

$$\phi(x) = \phi_{n_x-2} + c\left(x - x_{n_x-2}\right) + d\left(x - xn_x - 2\right)^2 \tag{3.80}$$

where ϕ_{n_x-2} is the potential at the grid point $x_{n_x-2} \equiv L - 2\Delta x$. For the grid points x_{n_x-1} and x_{n_x} we have the equations,

$$\phi_{n_x-1} = \phi_{n_x-2} + c\Delta x + d(\Delta x)^2 \tag{3.81}$$

and

$$\phi_{n_x} = \phi_{n_x-2} + 2c\Delta x + d(\Delta x)^2 \tag{3.82}$$

respectively, from which the constants ' c ' and ' d ' can be obtained as

$$c = -\frac{\phi_{n_x} - 4\phi_{n_x-1} + 3\phi_{n_x-2}}{2\Delta x} \tag{3.83}$$

and

$$d = \frac{\phi_{n_\alpha} - 2\phi_{n_\nu-1} + \phi_{n_\perp-2}}{2(\Delta x)^2} \tag{3.84}$$

The electric field near $x = L$ is obtained by taking the derivative of eq.3.80 as

$$\begin{aligned} E(x) &= -\frac{d\phi(x)}{dx} \\ &= -c - 2d\left(x - x_{n_x-2}\right) \end{aligned} \tag{3.85}$$

So that the electric field at the right-hand boundary is given by

$$\begin{aligned} E(x = L) &= -c - 4d\Delta x \\ &= -\frac{3\phi_{n_x} - 4\phi_{n_z-1} + \phi_{n_z-2}}{2\Delta x} \end{aligned} \tag{3.86}$$

(d) The Electric Field at any Point in the Simulation Region:

Once we have calculated the electric field at every grid point, the electric field at any point in the simulation region is obtained by linear interpolation between two nearest grid points x_j and x_{j+1} as,

$$E(x) = \frac{(x_{j+1} - x)E_j + (x - x_j)E_{j+1}}{\Delta x} \tag{3.87}$$

3.7 Iteration Scheme

Here, we are dealing with collisionless, time independent system only. The initial-guess potential, $\phi^{(0)}(x_j)$, is taken as input to the main iteration block, which will yield the first iteration to the potential distribution $\phi^{(1)}(x_j)$. With the new potential as input, the main iteration block will be invoked again yielding $\phi^{(2)}(x_j)$ until the potential distribution has converged in the sense outlined in fig. 3.2 below.

The boundary potentials $\phi(x = 0)$ and $\phi(x = L)$ and the boundary injection distribution functions $f^s(L, v)$ are to be provided as input parameters. Hence, they must be specified before entering the iteration scheme and are kept constant throughout the entire simulation. To start the scheme, we must suitably prescribe an initial-guess potential distribution. We restrict ourselves to potential distributions $\phi(x)$ which decrease monotonically from $\phi(L) = 0$ to $\phi(0) = \phi_o \leq 0$. The starting potential distribution is chosen to be a linear interpolation between the potential values at the boundaries.

Here, we described the main iteration scheme discussed in the fig. 3.2. The main iteration block carries out the m^{th} iteration (i.e. it calculates the new distributions $\phi^{(m)}(x_j)$) for given input potential distribution, $\phi^{(m-1)}(x_j)$, by performing the following three steps.

Step 1: The new electron density distribution $n^{e(m)}(x_j)$ is calculated analytically using particle density function. The new ion density $n^{i(m)}(x_j)$ is calculated by DFA approaches, the new ion

densities $n^{1(m)}(x_j)$ and $n^{2(m)}(x_j)$ are obtained by velocity-space integration of the new velocity distribution functions.

Step 2: From the new ions and electron densities obtained in step 1, the new space-charge density, $\rho^{(m)}(x_j)$, is calculated.

Step 3: the new potential distribution, $\phi^{(m)}(x_j)$, is obtained by solving the matrix eq.(3.70) numerically with the new space-charge density, $\rho^{(m)}(x_j)$, inserted on the right hand side.

The new potential distribution, $\phi^{(m)}(x_j)$, obtained in step 3 of the main iteration block is compared with the old potential distribution, $\phi^{(m-1)}(x_j)$, and we consider the convergence to be reached if at each point x_j the condition

$$|\phi^{(m)}(x_j) - \phi^{(m-1)}(x_j)| \leq \delta \tag{3.88}$$

is satisfied with δ as accuracy parameter.

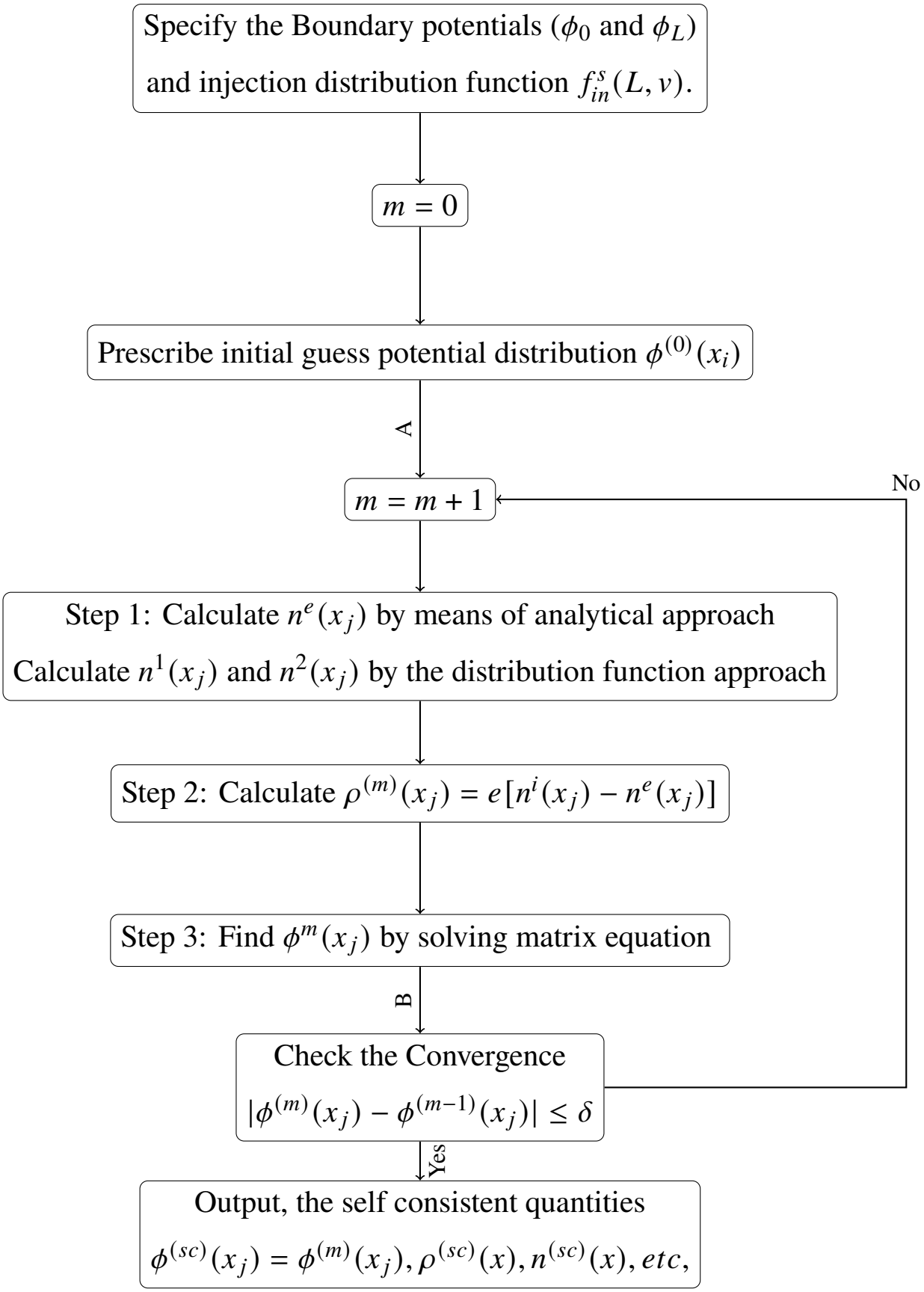

Figure 3.2: The iterative scheme used in kinetic trajectory simulation method

CHAPTER 4

RESULTS AND DISCUSSION

Chapter 4

Results and Discussion

In this chapter, result obtained for 1d3v plasma sheath simulation using solution of related kinetic equations for given boundary conditions for two positive ions has been discussed. Here, we have solved the dimensionless presheath-sheath coupling equations for given presheath parameter to obtain sheath side parameter. The positive ions presheath parameter is specified in the sheath entrance side $x = L$ and it gives ions trajectory to reach the wall $x = 0$ on solving kinetic equations using KTS model. Particle and field boundary conditions is used to initiate the simulation and observe effect of variation of ion temperature of both positive ions on multicomponent magnetized plasma sheath consists of two species of positive ions (i.e. Oxygen and Argon) and electrons. The considered numerical parameters value at the presheath side of the sheath-presheath boundary is set as length of region of interest (L) = $15\lambda_{De}$, magnitude of magnetic field (B) = 0.5T, obliqueness of magnetic field (θ) = 45^o, presheath electron temperature $(T^e_{ps}) = 5$ eV, presheath positive ions temperature $(T^i_{ps}) = (1 - 5)$ eV, plasma density $(n_{ps}) = 10^{15}$ m^{-3}, total number of space grid points $(n_x) = 41$, total number of trajectory $(n_{tra}) = 400$, total number of velocity grid points $(nv) = 300$, desired accuracy parameter for potential $(\delta\phi) = 10^{-6}$ V and relaxation parameter $\omega = 0.08$. The potential profile, particle (i.e. electron and ions) density profile, charge density profile and electric field profile for presheath temperature of heavier ion (1 eV) is less than that of smaller ion (5 eV), presheath temperature of heavier ion (1 eV) is equal to that of smaller ion (1 eV) and presheath temperature of heavier ion (5 eV) is greater than that of smaller ion (1 eV) taking fixed magnetic field strength and obliqueness is interpreted as follows.

4.1 Potential Profile

In figure 4.1, the variation of electric potential with normalized distance (x/λ_{De}) at constant magnetic field (B = 0.5 T) and fixed obliqueness ($\theta = 45^o$) is shown. For all the cases potential magnitude is smoothly increases towards wall from the injection boundary. When the heavier ion temperature (5 eV) is greater than that of smaller ion (1 eV), the magnitude of electric potential at the wall is slightly lower than the opposite case in figure 4.1 (a). But for equal ion temperature (i.e. 1 eV), the magnitude of electric potential is maximum and on increasing ion temperature of both ions equally, the electric potential is decreased in magnitude which can be seen in figure 4.1 (b). This is because of number density of ions reaching the wall is increased on increasing ion temperature which causes the declination of potential.

(a)

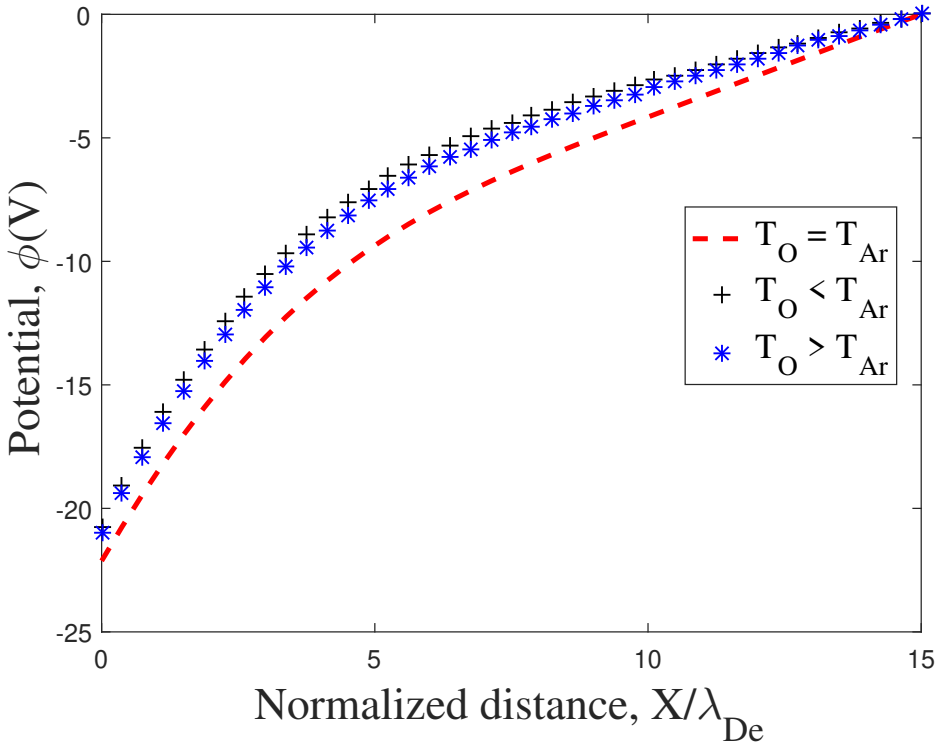

(b)

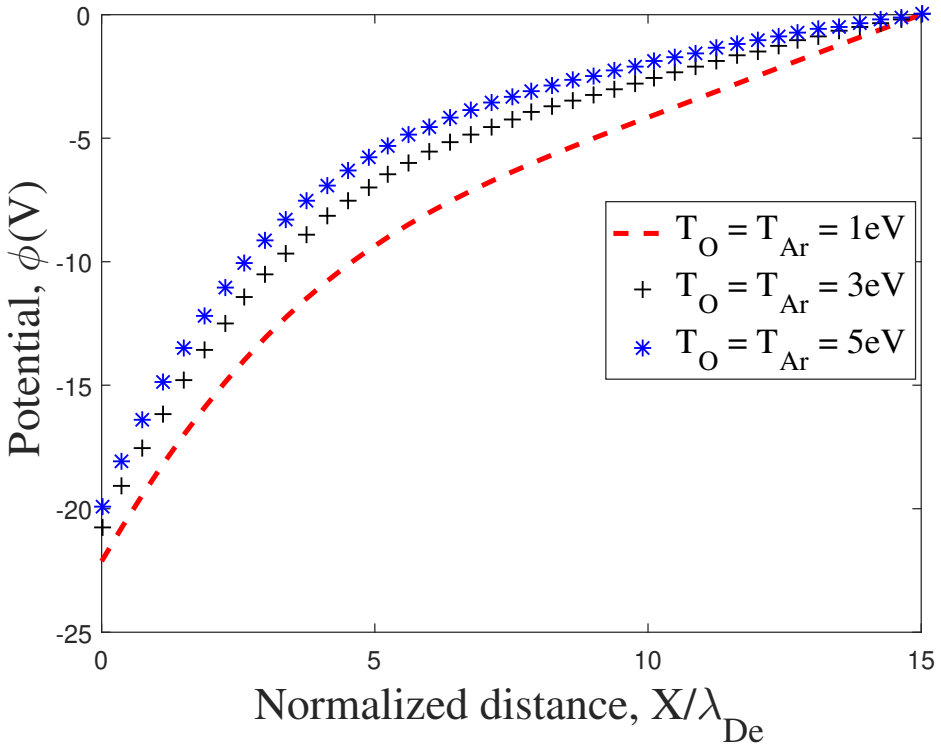

Figure 4.1: The variation of potential in the plasma-wall transition region for **(a)** different cases of ion temperature of both ions and **(b)** equal ion temperature of both ions.

4.2 Particle Density Profile

In figure 4.2, the variation of smaller ion density with normalized distance (x/λ_{De}) at constant magnetic field (B = 0.5 T) and fixed obliqueness ($\theta = 45^o$) is shown. For all the cases of ion temperature variation, smaller ion density is maximum at injection boundary and moves faster towards the wall and acquires maximum value (i.e. $8.906 * 10^{-2} n_{ps}$) at wall when we take the smaller ion temperature is greater than that of heavier ion , this is due to increase in the thermal velocity of that ion. But for opposite case, the ion density of smaller ion is gradually decreases towards the wall and reaches lower value (i.e. $3.144 * 10^{-2} n_{ps}$) than previous case because of having larger heavier ion temperature which favours heavier ion number density to increase near the wall.

(a)

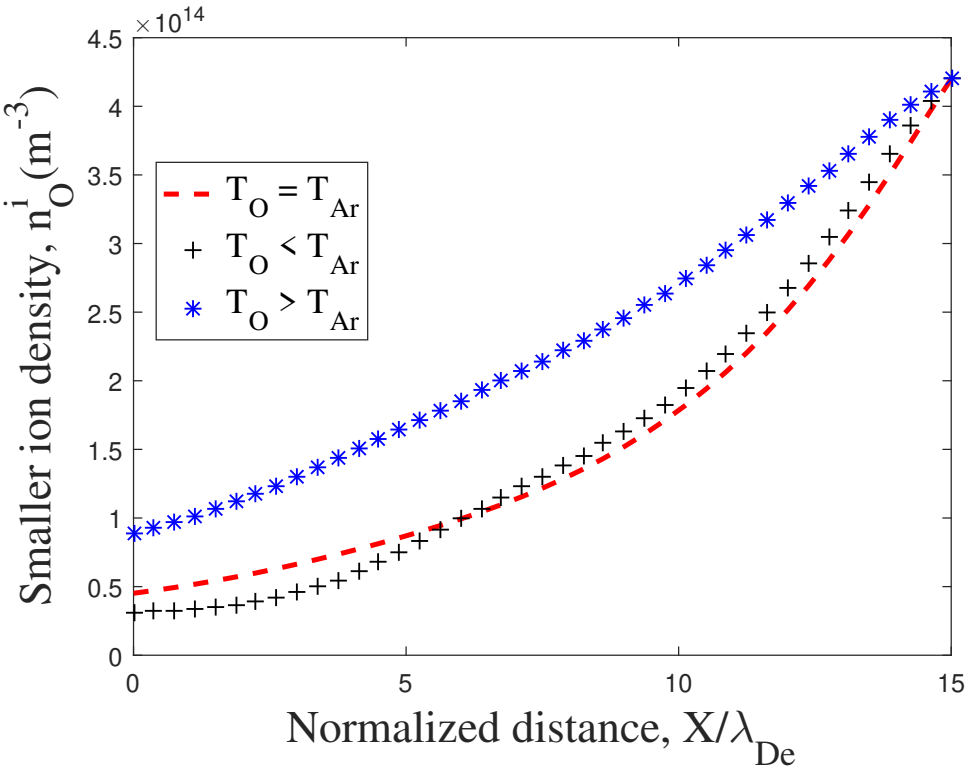

(b)

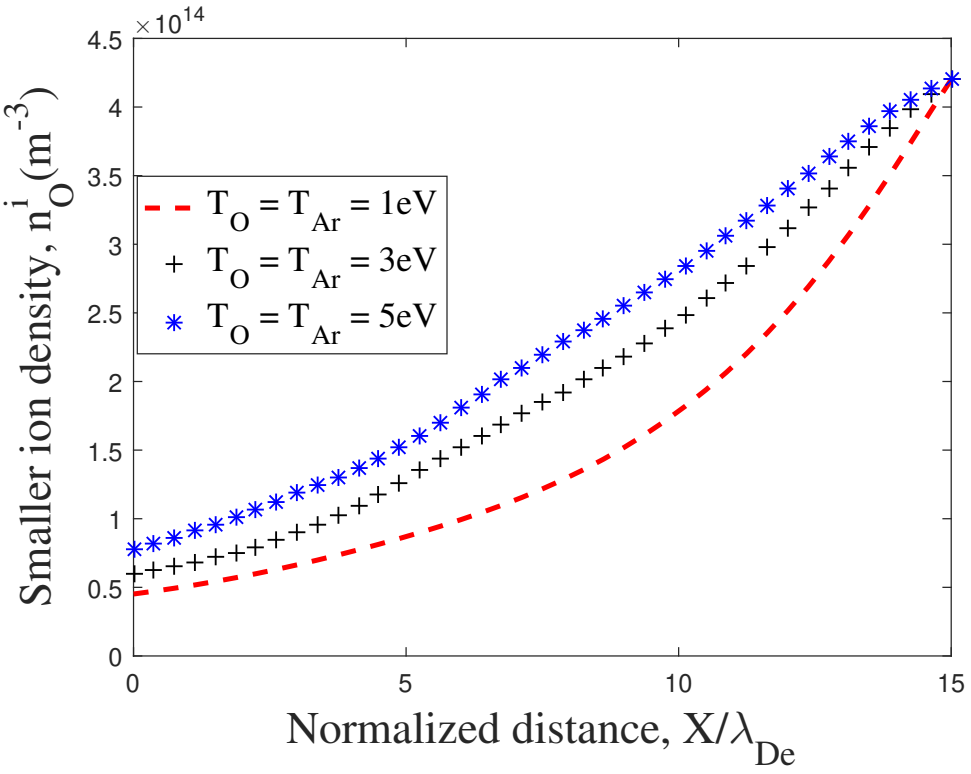

Figure 4.2: The variation of smaller ion density in the plasma-wall transition region for **(a)** different cases of ion temperature of both ions and **(b)** equal ion temperature of both ions.

In figure 4.3, the variation of heavier ion density with normalized distance (x/λ_{De}) at constant magnetic field (B = 0.5 T) and fixed obliqueness ($\theta = 45^o$) is shown. For all the cases of ion temperature variation, heavier ion density is maximum at injection boundary and sharply decreases towards the wall and acquires maximum value (i.e. $1.38 * 10^{-1} n_{ps}$) at wall when we take the heavier ion temperature is greater than that of smaller ion due to increase in thermal velocity of that ion which causes increased in ion flux towards the wall. But for opposite case, the ion density of heavier ion is gradually decreases towards the wall and reaches minimum value (i.e. $6.221 * 10^{-2} n_{ps}$) than previous case because of having greater value of smaller ion temperature.

(a)

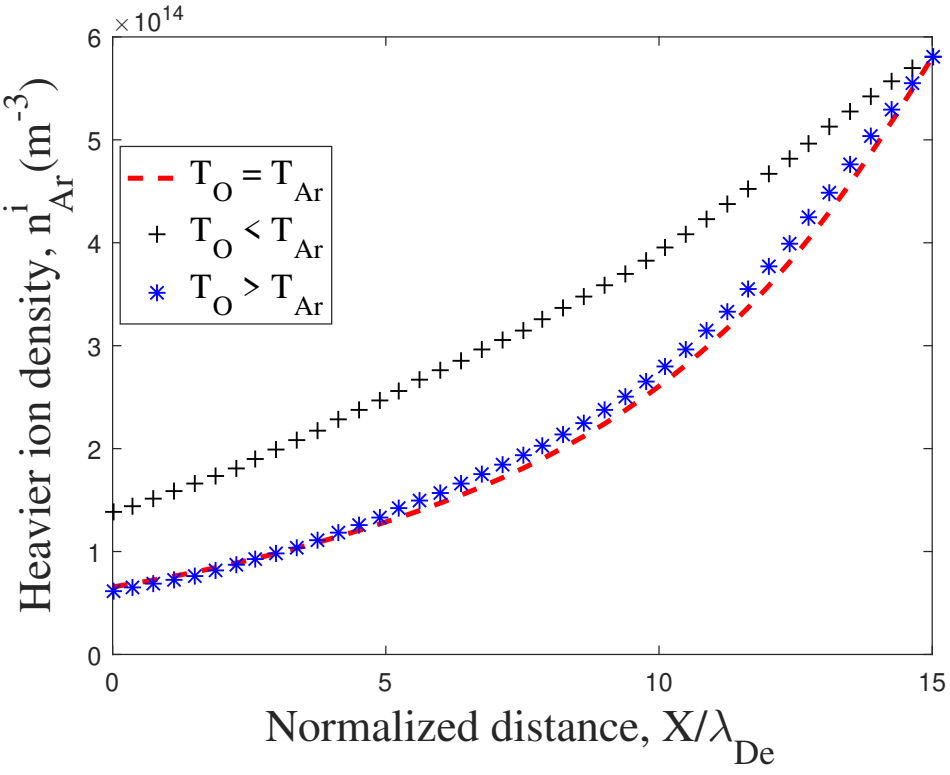

(b)

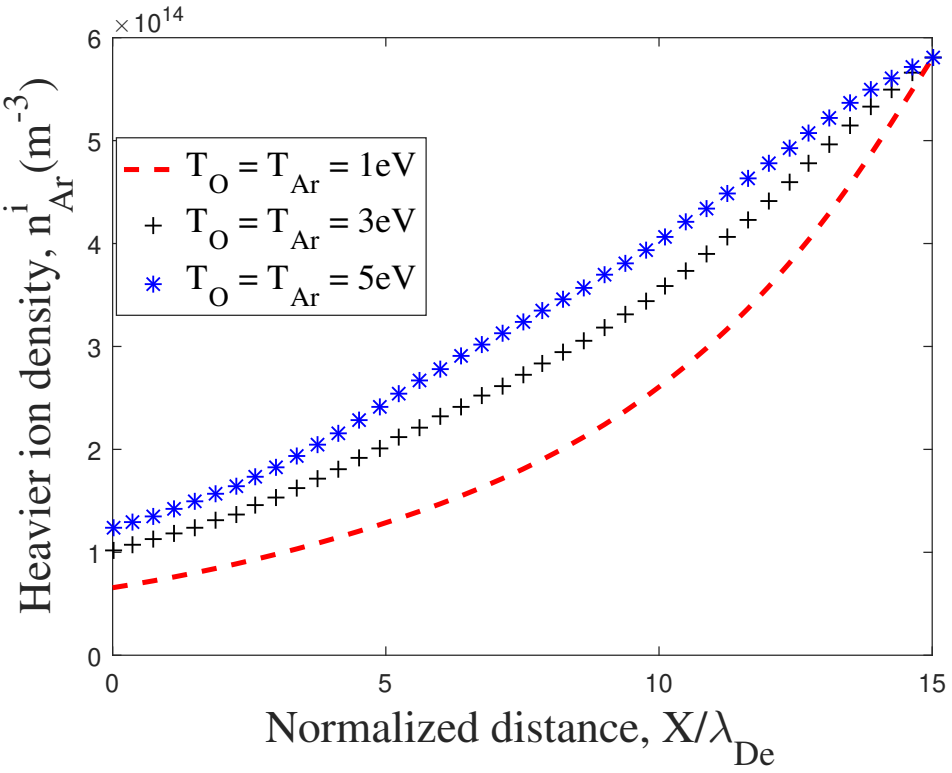

Figure 4.3: The variation of heavier ion density in the plasma-wall transition region for **(a)** different cases of ion temperature of both ions and **(b)** equal ion temperature of both ions.

In figure 4.4, the variation of electron density with normalized distance (x/λ_{De}) at constant magnetic field (B = 0.5 T) and fixed obliqueness ($\theta = 45^o$) is shown. For all the cases of ion temperature variation, electron density decreases gradually towards the wall and reaches its minimum value. When the ion temperature of heavier ion is greater than that of smaller ion, electron density in presheath-sheath region is slightly more than that in the case when smaller ion temperature is greater. The thermal velocity of electrons increases with the increase in temperature and reaches the wall fast which causes decrease in electron density.

(a)

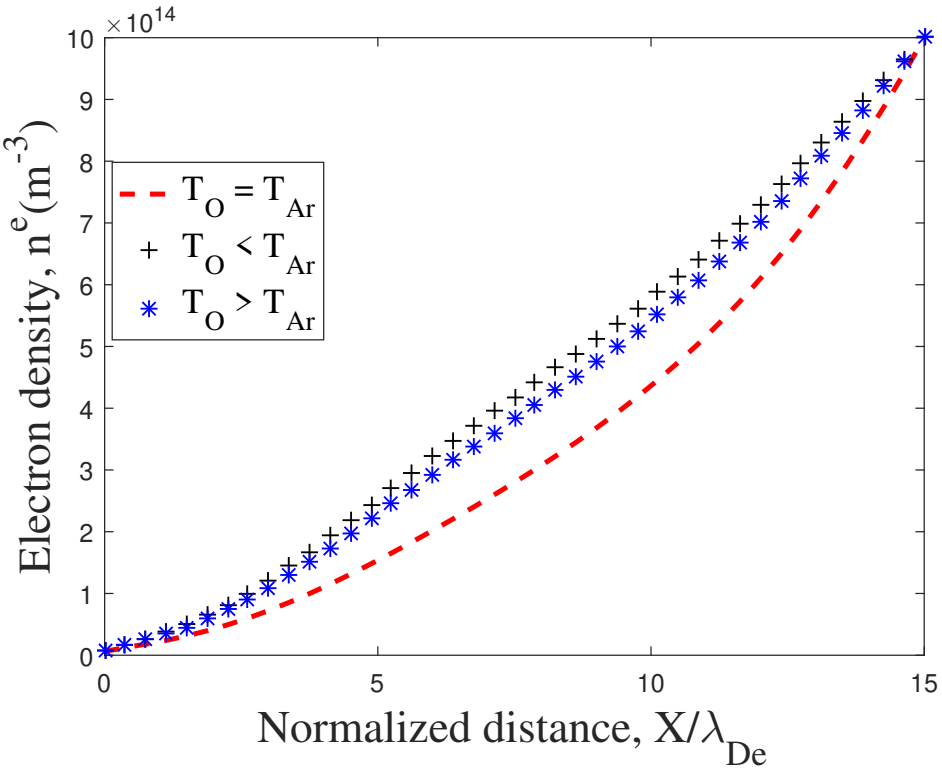

(b)

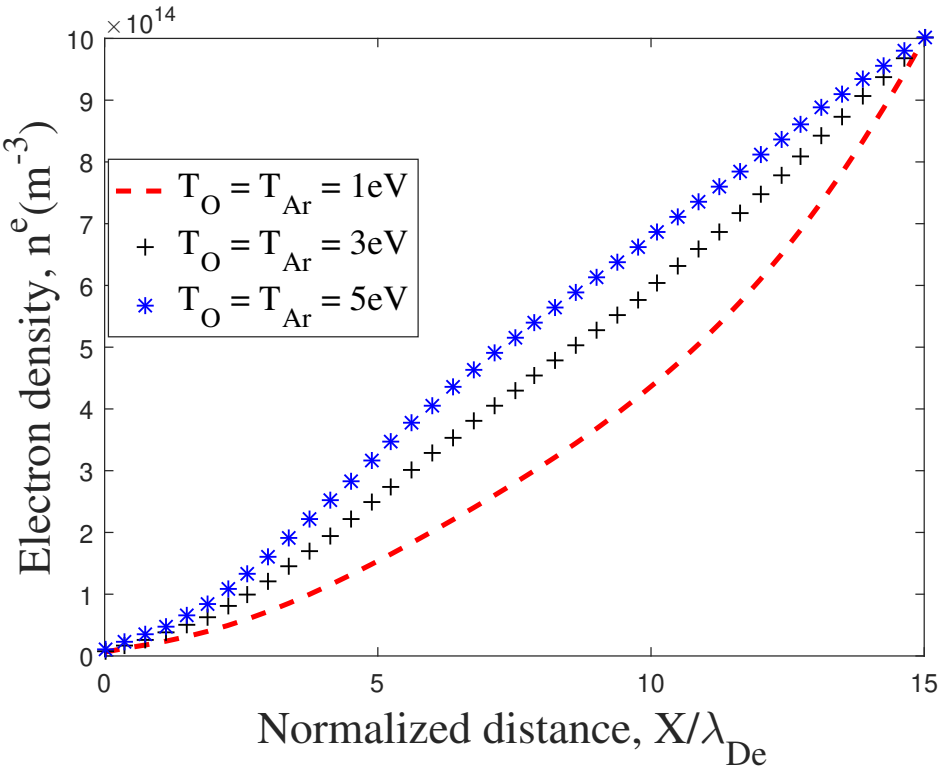

Figure 4.4: The variation of electron density in the plasma-wall transition region for **(a)** different cases of ion temperature of both ions and **(b)** equal ion temperature of both ions.

4.3 Electric Field Profile

Figure 4.5 shows the electric field (E_f) versus normalized distance (x/λ_{De}) at constant magnetic field (B = 0.5 T) and fixed obliqueness ($\theta = 45^o$) is shown for the three different cases of two positive ions. Electric field is always negative in the presheath-sheath region due to presence of negative potential. But its magnitude increases towards the wall moving from the sheath entrance. When the temperature of ions are changed in presheath the value of electric field also changes in sheath entrance because of low value of electric field required to trigger it when ion temperature value is high. When the Heavier ion temperature is 5 eV and smaller ion temperature is 1 eV then the value of electric field is small than other two cases and also its magnitude is increases slowly upto certain point and after that it leads the other to reach the wall then achieve maximum value in magnitude at wall. The magnetic field leads electric field upto certain Debye length after that the strength of magnetic field is less in comparison to electric field. Difference in magnitude of electric field at sheath entrance and the wall is minimum for equal ion temperature (i.e. 1 eV) of both ions and maximum for ion temperature (i.e. 5 eV) of heavier ion and (i.e. 1 eV) of lighter ions (i.e it goes through 878.6 Vm^{-1} to 8689.4 Vm^{-1} in magnitude). And for reverse case, its value increases from 1014.6 Vm^{-1} to 8309 Vm^{-1}.

(a)

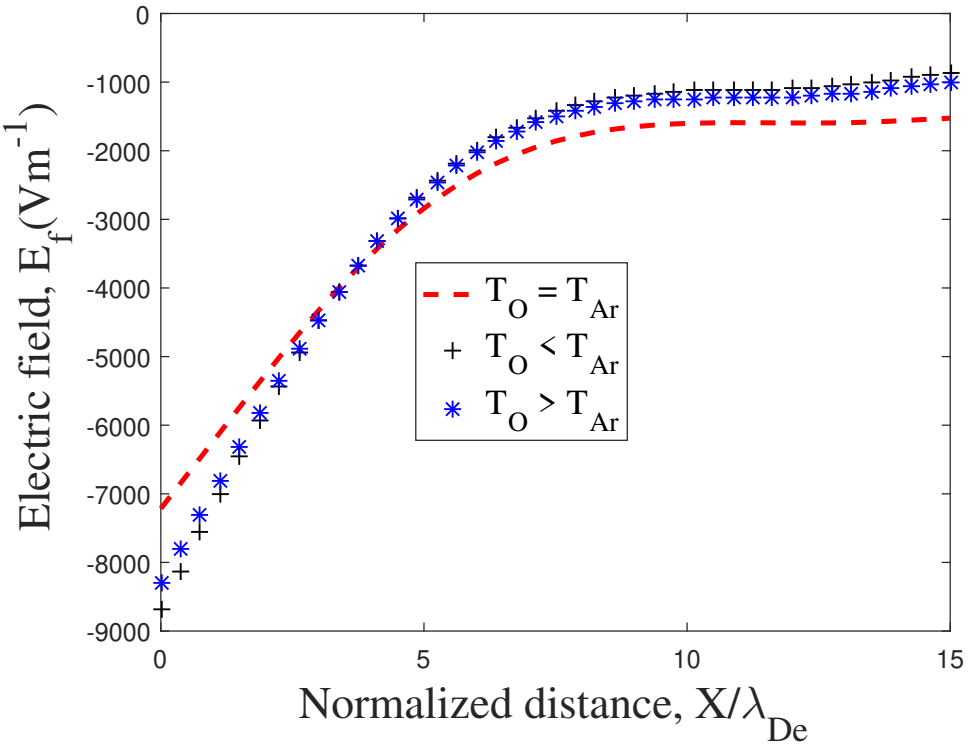

(b)

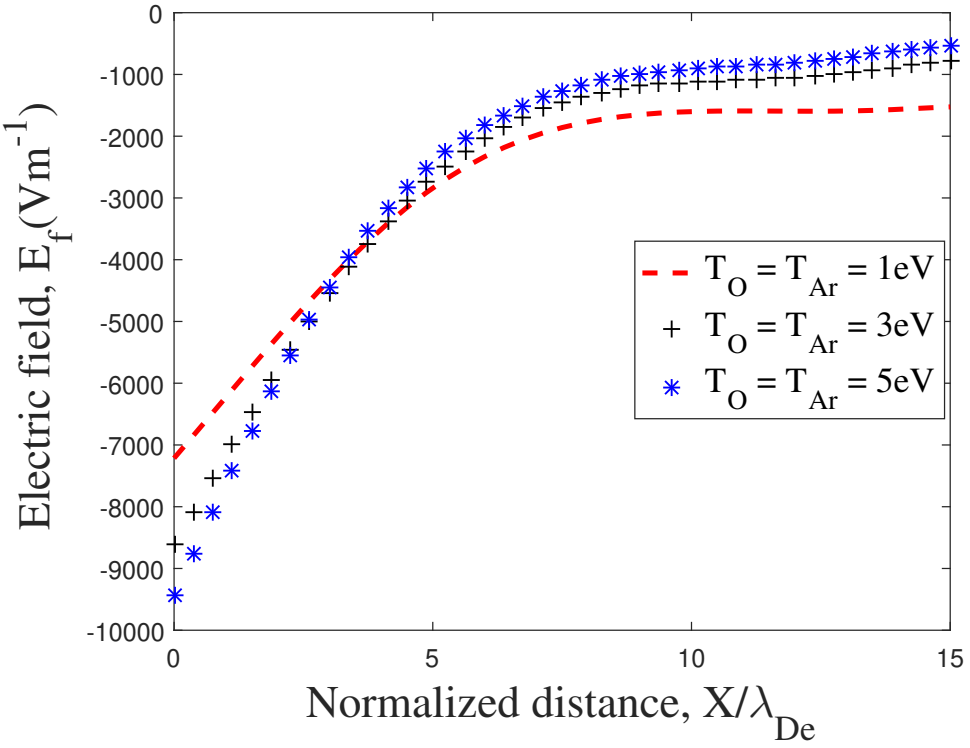

Figure 4.5: The variation of electric field in the plasma-wall transition region for **(a)** different cases of ion temperature of both ions and **(b)** equal ion temperature of both ions.

4.4 Space Charge Density Profile

In figure 4.6, the variation of space charge density (ρ) versus normalized distance (x/λ_{De}) at constant magnetic field (B = 0.5 T) and fixed obliqueness ($\theta = 45^o$) is shown for the three different cases of two positive ions. Initially, magnitude of space charge density is exactly zero at the particle injection boundary to retain quasineutrality of plasma in that region. Space charge density slightly increases after moving from sheath entrance towards the wall and then decreases from the sheath entrance to 10 Debye length and after that steeply increases towards the wall and obtains its maximum value due to rapid decrease in electron density at wall than ion density. As we take $T_O < T_{Ar}$, $T_O > T_{Ar}$ and $T_O = T_{Ar}$ the total charge density decreases on the wall due to decreasing the density of ions at the wall for these cases respectively shown in figure 4.6(a). On ascending the value of ion temperature of both the positive ions the magnitude of space charge density also increases shown in figure 4.6(b).

(a)

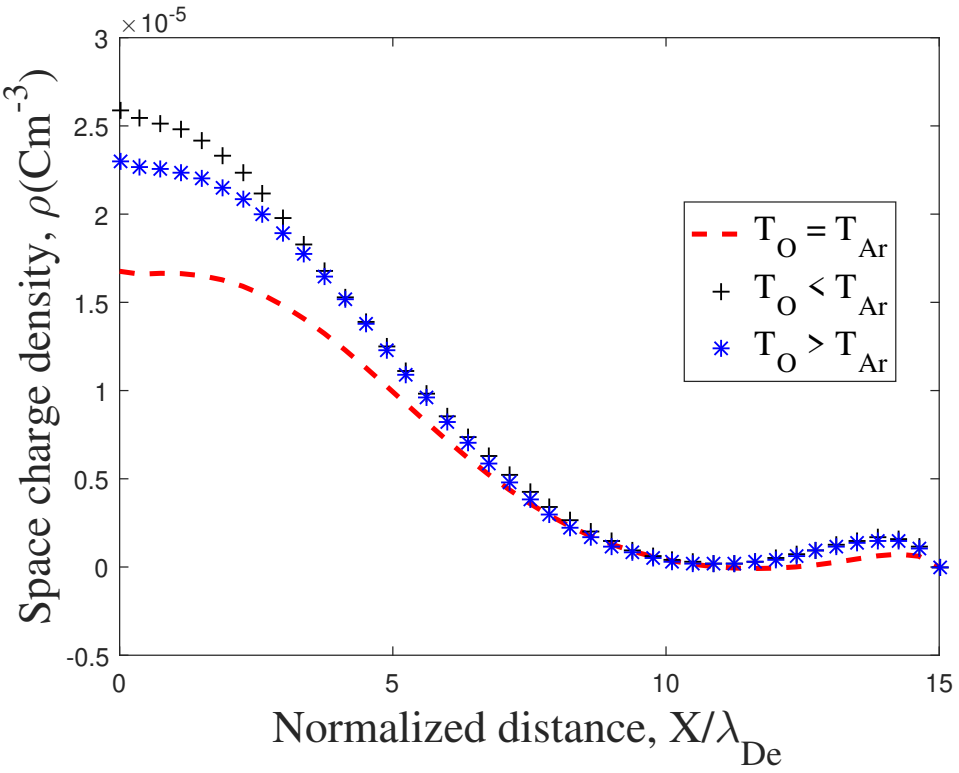

(b)

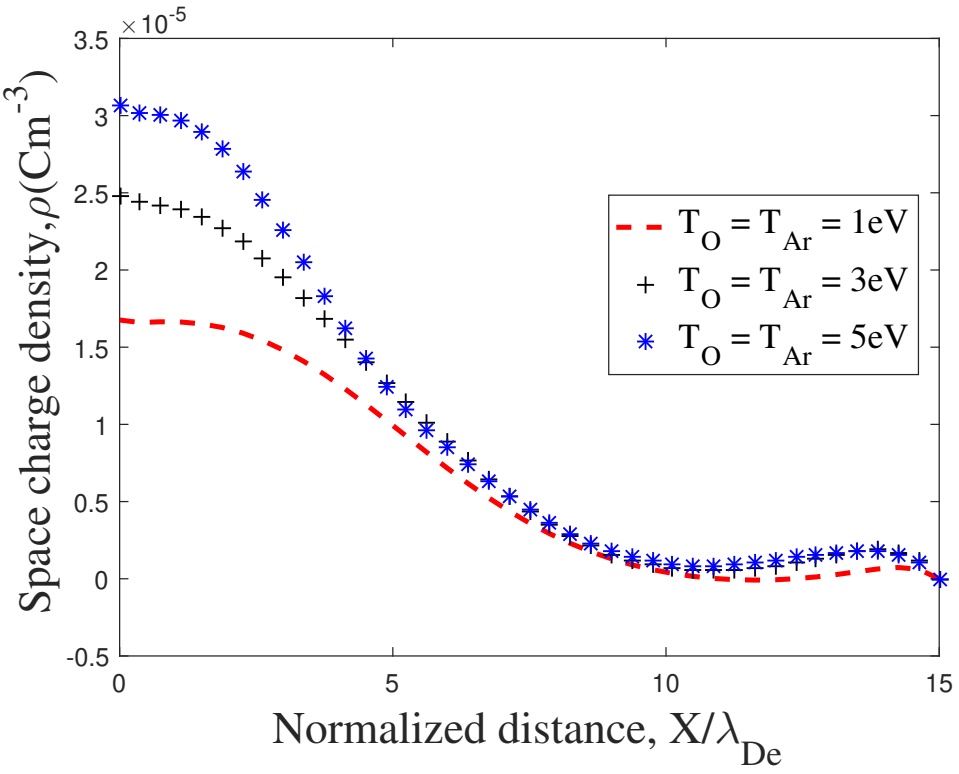

Figure 4.6: The variation of space charge density in the plasma-wall transition region for **(a)** different cases of ion temperature of both ions and **(b)** equal ion temperature of both ions.

CHAPTER 5

CONCLUSION AND FUTURE WORKS

Chapter 5

Conclusion and Future Works

5.1 Conclusion

Using a kinetic trajectory simulation method, effect of temperature variation on both ions of magnetized two positive ion species is observed. We assumed that, for the given presheath side parameters of the injection boundary, plasma must satisfy the quasineutrality condition, Bohm Chodura criterion, sheath edge singularity condition and continuity of first three moments. The calculation of sheath parameters at the sheath side of the sheath-presheath boundary are then obtained from the coupling scheme. It was found that the temperature changes of both ions affect the electric potential profile, particle density profile, space charge density profile and electric filed profile in PWT. In the electric potential curve, particle species reaches the wall faster on increasing the temperature of any positive ions from initial equal temperature state and also the particle species reaches wall slightly faster in the case of heavier ion temperature is increased than smaller ion. In the particle density profile, number density of all particle species decreased from the initial injection condition of plasma state, the ion density remains maximum for their respective higher ion temperature but electron density for all the cases decreases much faster than positive ions and hit the minimum value. Electric field is always goes increasing towards wall from injection boundary in magnitude because of domination of electric field over magnetic field after certain distance. Magnetic field dominates near the sheath entrance and electric field dominates close to the wall. The difference between value of electric field at entrance and wall is maximum when equal temperature of both the positive ions is taken and it begins to decrease on increasing temperature of one of the positive ions temperature. The increase in value of space charge density

from almost zero at injection boundary towards the wall and reaches maximum value due to rapid decrease in electron density value and significant number density of ions at wall for different ion temperature of both the positive ions (i.e. $\rho = n_{i1} + n_{i2} - n_e$).

5.2 Future Works

In the present work, the magnetized plasma sheath characteristics have been presented in the presence of two ions having different temperature using kinetic trajectory simulation model. The three different cases of ion temperature is taken for the study of sheath formation on the wall. This work can be extended further to study the magnetized plasma sheath by adopting the following cases:

1) collision effect can be included.

2) changing both temperature and obliqueness.

3) using 3d3v dimension.

REFERENCES

[1] R. J. Goldston and P. H. Rutherford, *Introduction to Plasma Physics*, Institute of Physics Publishing, London (1995).

[2] W. Crookes, *J. Franklin Inst.*, **108**, 305 (1879).

[3] F. F. Chen, *Introduction to Plasma Physics and Controlled Fusion (3^{rd} edition)*, Springer, Switzerland (2016).

[4] K. U. Riemann, *IEEE Trans. Plasmas Sci.* **23**, 709 (1995).

[5] S. Basnet, *Study of Multi-Component Magnetized Plasma-Wall Interaction Using Kinetic Trajectory Simulation (KTS) Method*, Ph.D. Thesis, Tribhuvan University, Kirtipur, Nepal (2021).

[6] I. Langmuir, *Phys. Rev.* **33**, 954 (1929).

[7] D. Bohm, *The Characteristics of Electrical Discharges in Magnetic Fields*, edited by A. Guthry and R. K. Wakerling, McGraw-Hill (1949).

[8] R. Chodura, *Phys. Fluids* **25**, 1628 (1982).

[9] K. U. Riemann, *J. Phys. D: Appl. Phys.* **24**, 493 (1991).

[10] D. L. Holland, B. D. Fried, and G. J. Morales, *Phys. Fluids B: Phys. Plasmas* **5**, 1723 (1993).

[11] A. K. Shaw, S. Kar and K. S. Goswami, *Phys. Plasmas* **19**, 102108 (2012).

[12] M. M. Hatami, B. Shokri and A. R. Niknam, *Phys. Plasmas* **15**, 123501 (2008).

[13] R. Paul, S. Adhikari, R. Maulik, S. S. Kausik and B. K. Saikia, *Phys. Plasmas* **27**, 063520 (2020).

[14] S. F. Masoudi and M. Khoramabadi, *J. Theor. Appl. Phys.* **5**, 307 (2015).

[15] L. Huiping, Z. Xiu and Q. Minghui, *Plasma Sci. Technol.* **16**, 633 (2014).

[16] R. Khanal, *A Kinetic Trajectory Simulation (KTS) Model for the Bounded Plasmas*, Ph.D. Thesis, Innsbruck University, Austria (2003).

[17] R. Chalise, *Study of Magnetized Plasma-Wall Transition in Oblique Magnetic Field*, M. Sc. (Physics) Dissertation, Tribhuvan University, Nepal (2011).

[18] S. Basnet and R. Khanal, *Plasma Phys. Control. Fusion* **61**, 065022 (2019).

[19] B. P. Pandey, A. Samarian and S. V. Vladimirov, *Plasma Phys. Control. Fusion* **50**, 055003 (2008).

[20] G. Sharma, S. Adhikari, R. Moulick, S. S. Kausik and B. K. Saikia, *Phys. Scr.* **95**, 035605 (2020).

[21] S. Basnet, A. Sarma and R. Khanal, *Phys. Scr.* **95**, 065601 (2020).

[22] B. R. Adhikari, S. Basnet, H. P. Lamichhane and R. Khanal, *AIP Advances* **9**(5), 055123 (2019).

[23] A. K. Shaw, S. Kar, K. S. Goswami, and B. J. Saikia, *Phys. Plasmas* **19**, 012120 (2012).

[24] R. Chaulagain, *Effect of Temperature Variation in Two-Ion Species Magnetized Plasma Sheath*, M. Sc. (Physics) Dissertation, Tribhuvan University, Nepal (2017).